Republic of Iraq
Ministry of Higher Education
and Scientific Research
Al-Nahrain University
College of Science
Department of Physics

Preparation and Characterization of the $Sn_xBa_4Ca_2Cu_{x+4}O_y$ and $Y_nBa_5Cu_{n+5}O_y$ Compounds

A Thesis

Submitted to the College of Science/Al-Nahrain University as a partial fulfillment of the requirements for the Degree of Master of Science in Physics.

By

Roaa Fakhri Hadi

B.Sc. 2010/ College Science / Kerbala University

Supervised by

Prof. Dr. EMAD K. Al-SHAKARCHI

July 2015 *Ramadan 1436*

بسم الله الرحمن الرحيم

﴿ وقُلِ اعْمَلُوا فَسَيَرَى اللَّهُ عَمَلَكُمْ وَرَسُولُهُ وَالْمُؤْمِنُونَ ﴾

صدق الله العظيم

التوبة – ١٠٥

Supervisor Certification

I certify that this thesis entitled **"Preparation and Characterization of the $Sn_xBa_4Ca_2Cu_{x+4}O_y$ and $Y_nBa_5Cu_{n+5}O_y$ Compounds"** was prepared by **"Roaa Fakhri Hadi"** under my supervision at the College of Science / Al-Nahrain University as a partial fulfillment of the requirements for the Degree of Master of Science in Physics.

Signature

Name: Dr.Emad K. Al-Shakarchi

Scientific Degree: Professor

Date: / / 2015

In view of the available recommendation, I forward this thesis for debate by the examination committee.

Signature:

Name: Dr. Thamir A.jabbar

Scientific Degree: Assist. Professor

Date: / / 2015

Committee Certification

We, the examining committee certify that we have read the thesis entitled **"Preparation and Characterization of the $Sn_xBa_4Ca_2Cu_{x+4}O_y$ and $Y_nBa_5Cu_{n+5}O_y$ Compounds"** and examined the student **"Roaa Fakhri Hadi"** in its contents and that is our opinion; it is accepted for the Degree of Master of Science in **Physics**.

Signature:
Name: **Dr. Tariq A. Alwan AL-Dhahir**
Scientific Degree: **Professor**
Date: / / 2015
(Chairman)

Signature:
Name: **Dr. Azhar Jawad Dawud**
Scientific Degree: **Assist. Professor**
Date: / / 2015
(Member)

Signature:
Name: **Dr. Muna Moussa Abbas**
Scientific Degree: **Assist. Professor**
Date: / / 2015
(Member)

Signature:
Name: **Dr.Emad K. Al-Shakarchi**
Scientific Degree: **Professor**
Date: / / 2015
(Member/**Supervised**)

I, hereby certify upon the decision of the examining committee.

Signature
Name: **Dr. Hadi M. A. Abood**
Scientific Degree: **Assist. Professor**
Title: Dean of the College of Science
Date: / / 2015

الإهداء

إلى من بلغ الرسالة وأدى الأمانة . . ونصح الأمة . . إلى نبي

الرحمة ونور العالمين . .

سيدنا محمد صلَّ الله عليه وآله وصحبه وسلم

Acknowledgement

"In the name of Allah, the Most Beneficent, the most Merciful"

I would like to express my hearties thanks to my supervisor Prof. Emad Al-Shakarchi for his guidance, patience, advice and devotions of time, throughout my research. He taught me how to be a researcher with his wonderful personality.

I would like to extend my thanks to all staff members of the department of physics. My gratitude also goes to all my friends for their encouragement and motivations.

Finally, I would like to thank my family for their unconditional care until I reach to this point, without their continuous supports and precious payers I could not have been able to finish my research. I know their blessing will always with me in all my endeavors and I dedicate this success to them. Thanks my beloved family.

Summary

The present study includes the preparation of $Sn_xBa_4Ca_2Cu_{x+4}O_y$ and $Y_nBa_5Cu_{n+5}O_y$ compounds with (x = 3, 4, 5, 6, 7) and (n=3, 5, 7) by solid state reaction (SSR) method. The study was to conclude the superconductor behavior of both compounds. The prepared samples were analyzed by Meissner effect primary, and the excess oxygen content was measured by using Iodomertric titration method. The samples characterized by XRD patterns with computer program that was used to determine the value of lattice constant, Scanning Electron Microscope (SEM), Energy dispersive X-ray spectroscopy (EDS) to study the grain morphology and also resistivity measurement was performed by Van der Pauw method to conclude the nature of behavior.

The resistivity measurement results of Sn-Ba-Ca-Cu-O system showed that the semiconducting behavior, increases with decreasing the temperature toward low temperature, the lowest and the highest normal resistivity were found at x=6 and at x=4, respectively. The system Y-Ba-Cu-O showed a superconductor behavior with high transition temperature, the T_c at n=3 of about (113.6 K), the sample prepared with n=5 has T_c=113 K, meanwhile the sample prepared with n=7 has T_c=105 K.

The x-ray analyses for $Sn_xBa_4Ca_2Cu_{x+4}O_y$ samples showed that the tetragonal structure, and the c-parameter increased by increasing the value of (x) until reach to maximum value at x=5 then return back decreasing at x=6 and 7. The x-ray diffraction analysis of the compound $Y_nBa_5Cu_{n+5}O_y$ has orthorhombic phase and when Y-atom concentration and the number of CuO_2 layer increased tend to increase b and c-axis.

The Scanning Electron Microscopy (SEM) results showed that the appearance of nanostructure in $Sn_6Ba_4Ca_2Cu_{10}O_{22}$ and $Sn_7Ba_4Ca_2Cu_{11}O_{24}$ samples in the range (100-300 nm), whereas the other samples of Sn-family

was a microstructure. On the other hand, the Y-358 had large grains randomly comparable with Y-5 5 10, Y-7 5 12 addition to absent the interfaces distances from Y-358. The results of EDS showed that the agreement of the peaks appeared with the theoretical values.

CONTENTS

LIST OF TABLES

LIST OF FIGURES

LIST OF SYMBOLS

The following list includes definitions of must of the symbols used:

symbol	Definition
T_c	Critical temperature
H_c	Critical magnetic field
J_c	Critical current density
μ_o	Vacuum Permeability
M	Magnetization
χ_m	The magnetic susceptibility
H	External magnetic field
B_{in}	Internal magnetic flux density
BCS-theory	Bardeen Cooper Schrieffer- Theory
ω_D	Debye frequency
$\hbar$	Phonon energy
n_s	The local density of superconducting curriers
J_s	The supercurrent density
λ_L	London penetration depth
ψ	Electron microscopic wave function
ξ	The coherence length
δ	Excess of oxygen content
ΔT	Transition width
Y-123	$YBa_2Cu_3O_{7+\delta}$
Y-358	$Y_3Ba_5Cu_8O_{18+\delta}$
Y-5 5 10	$Y_5Ba_5Cu_{10}O_{22.5+\delta}$
Y-7 5 12	$Y_7Ba_5Cu_{12}O_{27.5+\delta}$
YBCO	Y-Ba-Cu-O
SBCCO	Sn-Ba-Ca-Cu-O
BSCCO	Bi-Sr-Ca-Cu-O
Bi-2223	$Bi_2Sr_2Ca_2Cu_3O_{10+\delta}$
SEM	Scanning Electron Microscope
EDS	Energy Dispersive Spectroscopy

CHAPTER ONE

Introduction of Superconductivity

1.1 Introduction

Superconductivity is a phenomenon occurring in certain materials having zero electrical resistance at very low temperatures, characterized by exactly zero electrical resistance at a certain low temperature and the exclusion of the interior magnetic field and producing diamagnetic behavior (the Meissner effect).

Superconductivity occurs in a wide range of materials, including simple elements like tin and aluminium, various metallic alloys and some heavily-doped semiconductors. Superconductivity does not occur in noble metals like gold and silver, or in most ferromagnetic metals [1].

There are many applications of superconductor's materials

- Superconducting Transmission Lines: Since 10% to 15% of generated electricity is dissipated in resistive losses in transmission lines, the prospect of zero loss superconducting transmission lines is appealing. The prototype design of superconducting transmission lines happened at Brookhaven National Laboratory, represented by 1000 MW of power can be transported within enclosure of diameter 40 cm. This amounts to transporting the entire output of a large power plant on one enclosed transmission line. This could be a fairly at low voltage DC transmission compared to large transformer banks and multiple high voltage AC transmission lines on towers in the conventional systems. The superconductor used in these prototype applications is usually niobium-titanium, and liquid helium cooling is required [2].

- High T_c Power Applications: Power applications of high temperature superconductors would have the major advantage of being able to operate at liquid nitrogen temperature. The biggest barrier to their application has been the difficulty of fabricating these materials as wires and coils. Current development focuses on BSCCO and YBCO materials [3].

- Fault-Current Limiters: High fault-currents caused by lightning strikes are a troublesome and expensive nuisance in electric power grids. One of the near-term applications for high temperature superconductors may be the construction of fault-current limiters which operate at 77 K. The need is to reduce the fault current to fraction of its peak value is less than the cycle (1/60 sec). A recently tested fault-current limiter can operate at 2.4 kV and carrying current 2200 amperes. It was constructed from BSCCO material [3].

- In the medicine field, magnetic resonance imaging MRI machines is using superconductor magnets to create the necessary field used to see the body without having to perform surgery. Using superconductors would allow stronger magnets to be built, providing clearer pictures of various types of cells and tissues [4].

- Superconducting Motors: Superconducting motors and generators could be made with a weight of about one tenth of conventional devices for the same output. This is the appeal of making such devices for specialized applications. Motors and generators are already very efficient, so there is not the power savings associated with superconducting magnets. It may be possible to build very large capacity generators for power plants where structural strength considerations place limits on conventional generators.

In 1995 the Naval Research Laboratory demonstrated a 167 hp motor with high-Tc superconducting coils made from Bi-2223. It was tested at 4.2 K

and at liquid helium temperature, 28 K with 112 hp produced at the higher temperature [3].

- Superconducting Maglev Trains: While it is not practical to lay down superconducting rails, it is possible to construct a superconducting system onboard a train to repel conventional rails below it. The train would have to be moving to create the repulsion, but once moving would be supported with very little friction. There would be resistive loss of energy in the currents in the rails. Ohanian reports an engineering assessment that such superconducting trains would be much safer than conventional rail systems at 200 km/h [5]. A Japanese magnetically levitated train set a speed record of about 321 mi/h in 1979 using superconducting magnets on board the train. The magnets induce currents in the rails below them, causing a repulsion which suspends the train above the track.

Promising future industrial and commercial applications include transformers, power storage, propulsion systems for vehicles such as ships and space cult, electric motors, particle accelerators, rotating machinery and microwave filters e.g., for mobile phone base station [6].

1.2 History of superconductors

Each event in science and technology has a historical sequence since its discovery and update. The superconductivity concept has a suitable sequence in the events since 1908, the time of discovery.

The first noticed of the superconductivity was by Onnes in 1908, initiated by the field of low-temperature physics by liquefying helium in his laboratory at Leiden. Three years later he found that below 4.15 K of the DC resistance of mercury dropped to zero, that time was the born of the field of superconductivity. Later, Onnes discovered that the application of a

sufficiently strong axial magnetic field restored the resistance to its normal value [7].

A breakthrough came in 1933 when Meissner and Ochsenfeld [8] showed that in magnetic fields below a certain threshold value the flux inside the superconductor was expelled, and that was defined a new thermodynamic state and no consequence of infinite conductivity. The phenomenon became known as the Meissner effect, and laid the foundation for a thermodynamic treatment of superconductivity [9].

In 1935 London's brothers showed that the Missner effect was a consequence of the minimization of the electromagnetic free energy carried by superconducting current [10].

The first theoretical concept represented by Ginzburg and Landau in 1950, which described superconductivity in terms of order parameter and provided a derivation for the London equations. In the same year it was predicted theoretically by Fröhlich (1950) that the transition temperature would decrease as the average isotopic mass increased.

It was called the isotope effect that was observed experimentally in the same time. The isotope effect provided support for the electron–phonon interaction mechanism of superconductivity [7].

In 1957, three scientists Bardeen, Cooper, and Schrieffer was formulated a systematic theory of superconductivity. They explained the nature of this phenomenon, it is a serious attempt to solve the mystery of superconductivity; this theory showed that under some circumstances, the electrons are coupled together by quantization phonon energy. This electron pair (Cooper Pair) flow through the lattice and cause the superconductivity. They awarded the Noble prize at 1972 [11].

In 1962, Josephson made the important theoretical prediction that a supercurrent can flow between two pieces of superconductor separated by thin

layer of insulator, where it can experience tunneling of Cooper pairs of electrons through the junction. The Cooper pairs on each side of the junction can be represented by a wave function similar to a free particle wave function. This phenomenon, now called the Josephson effect, is exploited by superconducting devices such as SQUIDS [12].

The highest transition temperature was recorded at 1973, of about 23.3 K. That was proved for new compound represented by a composite between niobium and germanium with different ratio [12]. That was considering the first superconductor components. It was an important rule for opening the way for new superconductor components produced later. The method of preparation and the optimization condition were the points in view in the preparation another new superconductor components up to getting high temperature superconductor components.

In 1986 Bednorz and Mueller made the remarkable discovery of superconductivity that brought an entirely new class of solids with an unbelievably high value of T_c = 35 K to the world of physics and materials science. A new superconducting material was La_2CuO_4 in which the ions of Ba^{+2}, Sr^{+2} or Ca^{+2} were substituted to replace some of La^{+3} ions and hole-carriers are created [13, 14].

Soon after this discovery, T_c goes to 90 K when La^{+3} ions were replaced by Y^{+3} ions in a superconducting compound of $YBa_2Cu_3O_{7-\delta}$ with a certain defect of oxygen atoms was made [14,15]. The reason for that was related to the presence of vacancies which play an important role in the mechanism of superconductivity. These vacancies produced due to the non-stoichiometry in the cations and anions with in the unit cell.

In 1988, Maeda et al. and Sheng et al announced the discovery for new family of copper oxide superconducting materials recorded higher T_c; it has

led to discover Bi–Sr–Ca–Cu–O and Tl–Ba–Ca–Cu–O compounds. They have T_c value of about 110 K and 125 K, respectively [16, 17].

The historical development of superconducting critical temperature is appeared schematically in Figure (1-1). It is clear that the jump in T_c was happened at 1986, the time of appearing high temperature superconductor.

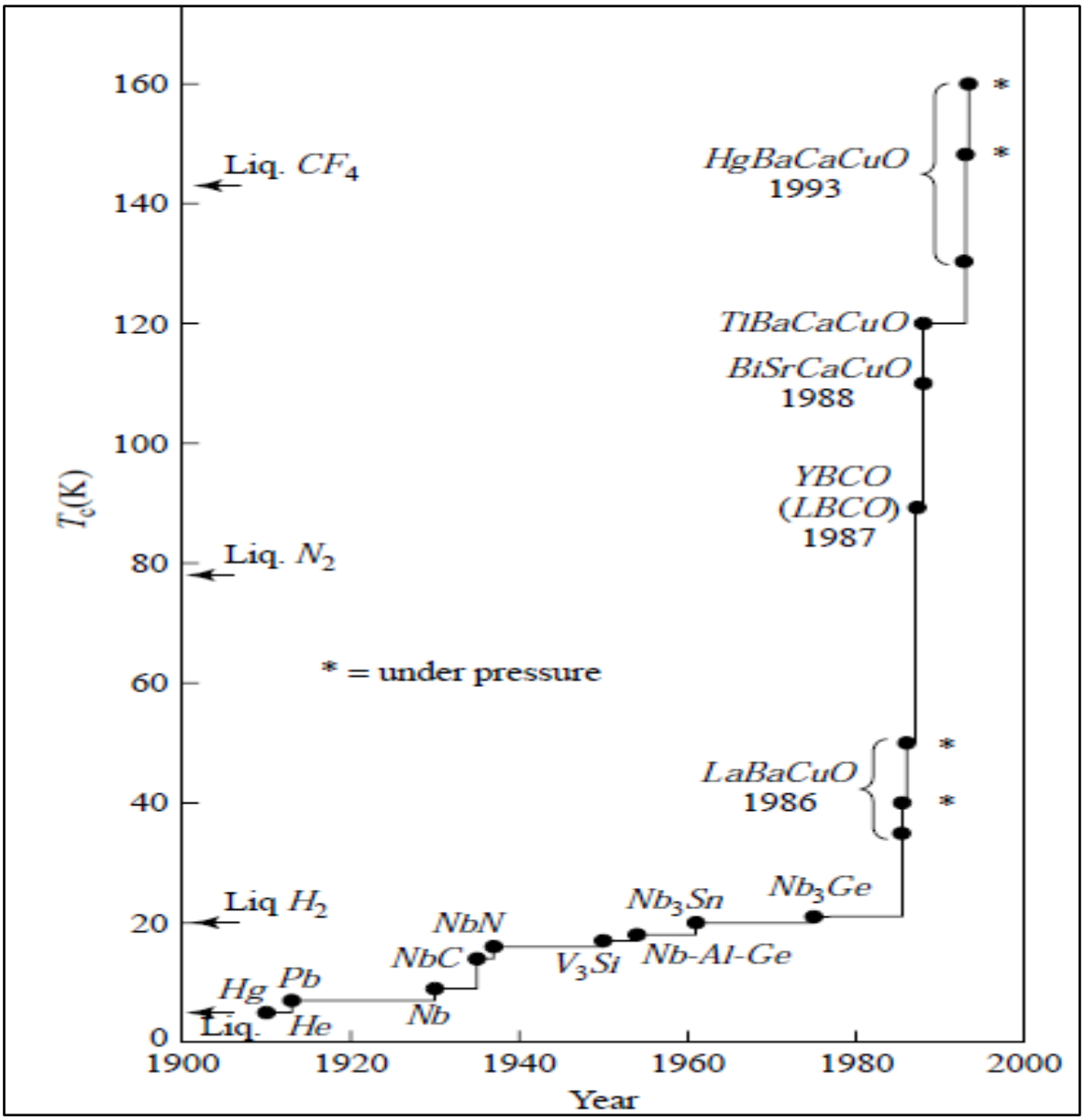

Figure (1-1): The historical development for different superconducting materials [14].

1.3 Superconducting parameters

The concept of superconductivity is a state that the electrical resistivity of a material suddenly drops to zero as soon as the temperature of material is brought down below a certain temperature.

The superconducting states determined by three parameters are the critical temperature T_c, the critical magnetic field H_c, and the critical current density J_c. If any of these three values is exceeded in some way their critical value, the material loses its superconductivity as shown in Figure (1-2) which illustrates the superconducting state as a region beneath a shaded (critical surface) [18].

1.3.1 Critical temperature (T_c) and zero resistivity

The superconducting state appears when many metals and alloys are cooled down to low temperature showing a special behavior called superconductivity. This temperature which is characteristic of the specific material called transition temperature or critical temperature [19].

1.3.2 Critical Magnetic Field (H_c)

There is another parameter doing as a shielding parameter of applied field on the superconductor materials. If the magnetic field is increased to a given point the superconductor will go to the normal state. The maximum value of the magnetic field applied at a given temperature is known as the critical magnetic field which given the symbol H_c [18].

1.3.3 Critical Current Density (J_c)

The third important parameter of any superconductor, from the point of view of practical applications, is the maximum electrical transport current density that the superconductor is able to maintain without resistance [20]. It is considering the shielding parameter also.

The minimum current that can pass through the sample without destroying its superconductivity is called the critical current I_c. This is known as silibees' rule, such that if $I > I_c$ then the material goes to normal state [21].

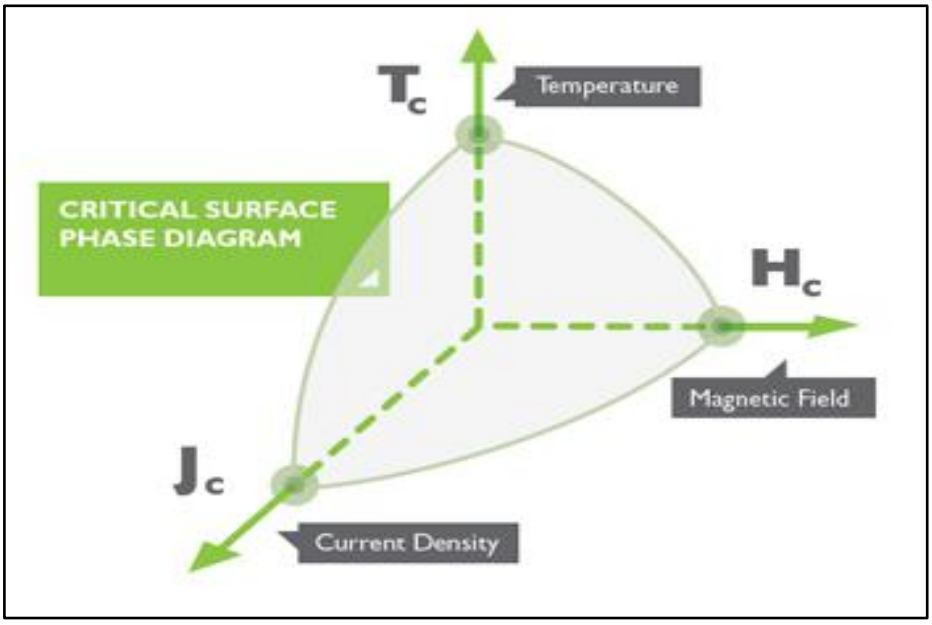

Figure (1-2): The superconductivity phase diagram

1.3.4 Meissner effect

When a superconducting material is cooled down below its critical temperature, it expels all magnetic flux from within its interior as shown in Fig. (1-3), i.e. the magnetic flux (B), is zero inside a superconductor. Meissner and Ochsenfeld managed to escape this conceptual trap by observing that a magnetic field, which was applied above T_c would be expelled from the body of the superconductor by cooling below T_c, leading to B = 0 inside it [9].

According to Lenz's law a current would be generated, which would oppose the flux, and reject any magnetic field from the superconductor. The magnetic induction inside the substance is given by [22, 23]:

$$B_{in} = \mu_o H + \mu_o M = 0 \quad (1.1)$$

$$= \mu_0 H + \mu_0 H \chi_m \quad (1.2)$$

$$= \mu_o H (1+\chi) \quad (1.3)$$

Because there is no magnetic field inside the specimen, B=0, then the superconductor in magnetic field will act as a perfect diamagnetic, because (χ = - 1).

Where μ_o: permeability of free space

M: magnetization of the medium

χ: the magnetic susceptibility

H: external magnetic field

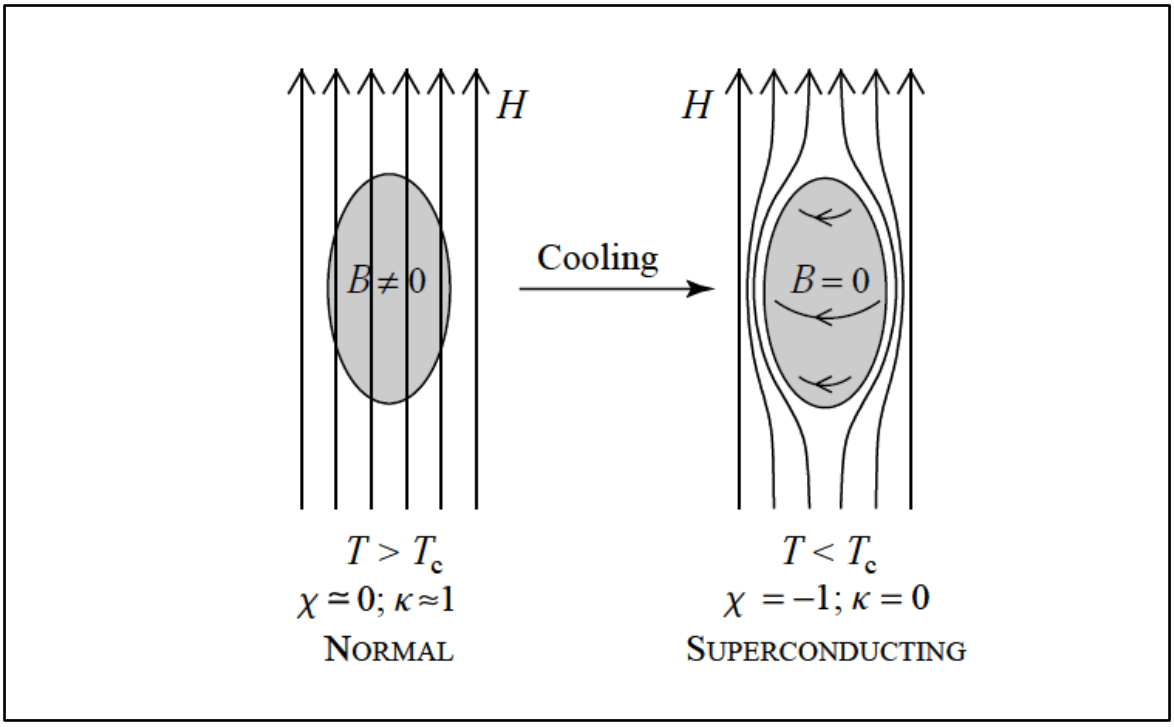

Figure (1-3): The Meissner effect in a superconductor [14].

1.4 London Equations

The brothers F. and H. London [24] stated the electrodynamics behavior of a superconductor. The London equations derived by Maxwell's equations, they demonstrated that an applied magnetic field **B** does not drop to zero abruptly inside the superconductor but penetrates to a certain depth. These two fundamental electrodynamic features were well expressed by them with two equations dealing with the electric and magnetic fields:

$$\frac{\partial}{\partial t} J_s = \frac{n_s e^2}{m} E = \frac{1}{\mu_0 \lambda_L^2} E \quad (1.4)$$

$$\nabla \times J_s = -\frac{1}{\mu_0 \lambda_L^2} B \quad (1.5)$$

$$\lambda_L = \sqrt{m/(\mu_0 n_s e^2)} \quad (1.6)$$

Where n_s is the number of superelectrons per unit volume, m and e their mass and electric charge, respectively, μ_0 the permeability in vacuum, λ_L penetration depth [25].

The magnetic field decreases exponentially as one proceeds from the surface into the superconductor. That means there is a small region with a thickness (λ_L) near the surface in which there is an appreciable field this parameter is known as "The London Penetration Depth" as shown in Figure (1-5). The parameter (λ_L) increases from absolute zero up to λ_L as T increases as the following [18, 26]:

$$\lambda_L = \lambda_L(0) + \left[1 - \left(\frac{T}{T_C}\right)^4\right]^{-1/2} \quad (1.7)$$

Where $\lambda_L(0)$ is the penetration depth at T=0 K. The penetration depth goes to infinity at $T=T_c$, therefore the material became in normal state.

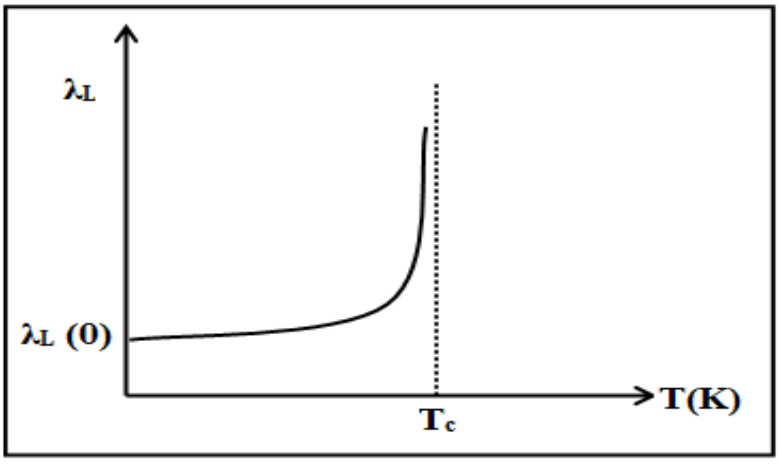

Figure (1-4): The penetration depth λ_L changes with the temperature [27].

1.5 Ginzburg-Landau (G-L) Theory

Ginzburg and Landau proposed a generalization of the London equations, introducing a complex wavefunction $\psi(r)$ also called a G–L wave function of the condensate state. It was used to describe the superconducting state and return to wave function of electron within the normal state. Which they concluded a new parameter called a coherence length (ξ) to investigate the thermodynamic properties of an interface between super and normal conductors [23, 28]. G-L theory also argues that ψ is related to the density of superelectrons, n_s, such that [18, 29]:

$$|\psi(r)|^2 = n_s \qquad (1.8)$$

The basic assumptions of the G–L theory were dependent in the analysis the presence of superconductor as following [24]:

• There is a single wave function $\psi(r)$ for the condensate state, which is in complex and depends on the position of bosonic field**.**

• It is absolute square is normalized to the density of the condensate state: $|\psi(r)|^2\ d^3r$= the number of condensed state.

• The $\psi(r)$ cannot change appreciably within the coherence length.

1.6 BCS – Theory

The scientific concept of BCS theory that was developed by Bardeen, Cooper and Schrieffer [25] depends on the quantum mechanic treated to superconductivity. The microscopic model BCS theory successfully describes all properties of superconductors such as: attractive effective electron-electron interaction to form Cooper pairs, role of lattice vibrations, and predicts transition temperature below which the superconductivity occurs [11, 18].

The pairs form because of some attractive interaction between the electrons. The condition for this interaction is done by the presence of phonon

energy. The superconducting properties arise from the fact that the cooperative condensed state acts in many ways as a single macroscopic quantum state, or wave function of the superelectrons [19, 30]. This wave function is applied by the bosonic field. The bosonic field is created by the interaction of electron-electron pairs.

The electrons interact attractively indirectly in the following way: one electron slightly disturbs the lattice in its neighborhood. The resulting phonon interacts quickly with another electron, which takes advantage of the deformation and lowers its energy. The second electron should be coupled by a phonon absorbed by lattice vibration tend to interact with the first electron producing cooper pairs. It is that passing back and forth of phonons which couples the two electrons together and brings them into a lower energy state. Electrons in such a Cooper-pair as shown in Figure (1-4) are situated on the Fermi surface and have opposite momentum and opposite spin [31, 32].

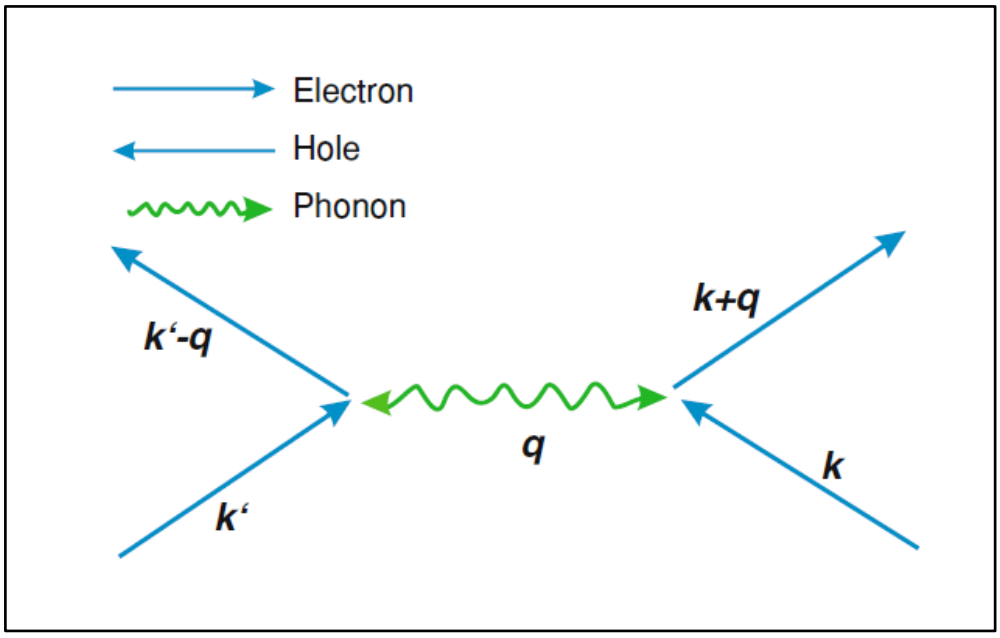

Figure (1-5): Diagrammatic representation of the effective electron–electron interaction through the exchange of a phonon q [33].

The BCS theory allows investigating a several features such as the transition temperature to superconducting state and the gap in the one-particle excitation spectrum. In their theory, the following approximations were made:

a. The pairing interaction is weak.

b. The density of states is not varying too fast near the Fermi surface.

c. The pairing interaction is constant and independent of momentum ($V_{qk} = V_o$) within the cutoff frequency $\pm\hbar\omega_D$ near the Fermi surface, where ω_D is the Debye frequency.

These approximations lead to conclude the BCS equations for the transition temperature T_c and the superconducting gap(Δ):

$$T_C = 1.14\hbar\omega_D \exp\left(-\frac{1}{N(E_F)V_0}\right) \quad (1.9)$$

$$\Delta = 2\hbar\omega_D \exp\left(-\frac{1}{N(E_F)V_0}\right) \quad (1.10)$$

Where $N(E_F)$ is the electronic density of states inside the Fermi surface. Since the pairing interaction is constant, the gap has isotropic s-wave symmetry [28, 33].

1.7 Types of superconductors

The interior of a bulk superconductor divided into two types depending on the mechanism of the magnetic field penetration. There are other parameters for this division related to the value of Tc and the nature of superconductor materials. If it is elemental superconductor means type I superconductor whereas the compound superconductor showed type II superconductor. The conclusion of G-L theory with the results of BCS-theory exhibited the presence of two important parameter, order parameter (κ) and coherence length. All these parameters have a direct effect on the classification of two superconductor types.

1.7.1 Type – I superconductors

Superconductor materials classified according to the value of G-L results. When the parameter $\kappa = \lambda/\xi$, If $\kappa < 1/\sqrt{2}$ the superconductor is classified as type-I [23]. This type is normally exhibited in pure element superconductor, like aluminum, lead, and mercury. The superconductor switches abruptly by Meissner effect that means the magnetic susceptibility goes to (-1), at a well-defined critical field H_c [9].

1.7.2 Type – II superconductors

When the order parameter $\kappa > 1/\sqrt{2}$ the superconductor is classified as type-II. It is usually made of metal alloys or complex oxide ceramics such as Nb_3Sn, NbTi, and all high-T_c cuprates. The superconductors have partial penetration of magnetic flux at a certain applied magnetic field (H_c). There is a mixed state at a range of (H_{c1}-H_{c2}) critical field. Thereafter it crosses over continuously to full flux penetration, the normal state, at an upper field H_{c2} [32]. These two type are shown in Figure (1-6).

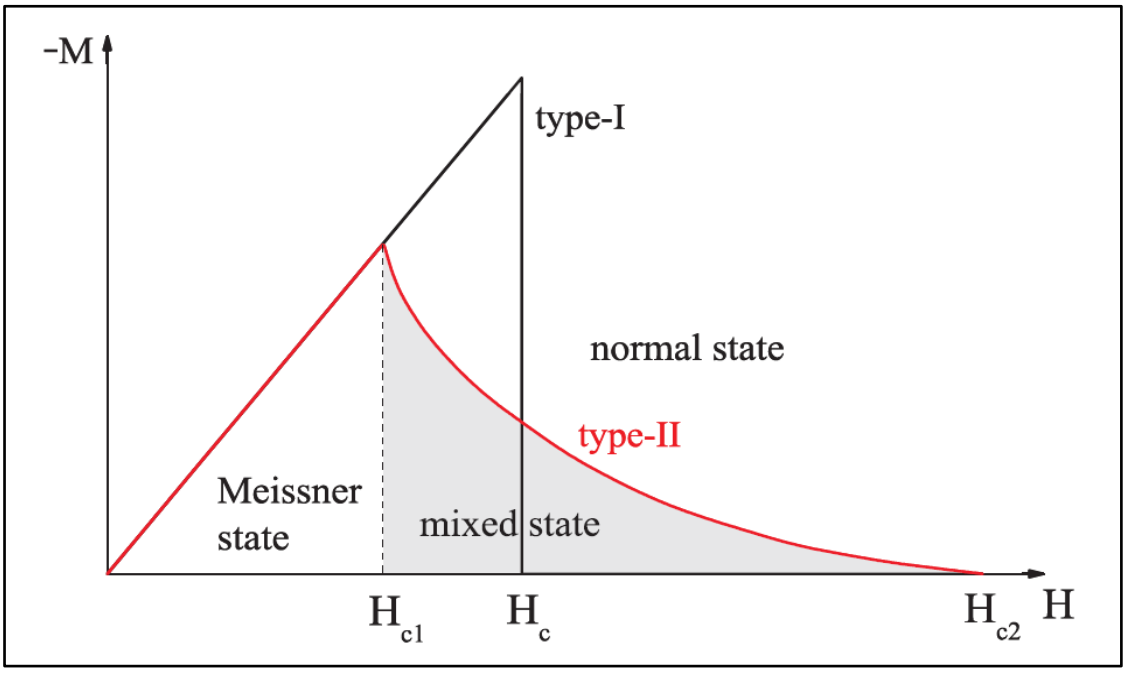

Figure (1-6): The magnetization as a function of the applied magnetic field of bulk type-I and type-II superconductor [32].

1.8 Literature Review of Sn-family

The main objective of this work is to examine two types of compounds. There is a predication that both are superconductor depends on the limited literature review.

Aleksandrov et al [34], synthesized $SnBaSrCu_3O_x$, $SnBaCaCu_3O_x$, $SnBaMgCu_3O_x$, $SnSrCaCu_3O_x$, $SnSrMgCu_3O_x$, and $SnCaMgCu_3O_x$ by using multistep ceramic procedure at 960 ^oC for 12 h. The $SnBaSrCu_3O_x$ compound exhibited normal resistivity about 10 Ω.cm, while the other compounds were insulators with normal resistivity larger than 1000 Ω.cm. Then they substituted a partial of K^{+1} and Y^{+3} for the divalent barium and strontium cations, $SnBa_{0.7}Sr_{0.7}K_{0.7}Cu_3O_x$ and $SnBa_{0.7}Sr_{0.7}Y_{0.7}Cu_3O_x$. The first compound was turned out to be a typical paramagnet; the second compound was exhibited magnetic and electrical properties refer to superconducting phase. They also studied the $SnBa_2Sr_{0.5}Y_{0.5}Cu_3O_x$ compound and found that it had well-expressed superconducting properties. The spectra analysis of this compound suggests that it retains the same basic structural motif of $YBa_2Cu_3O_7$, the unit cell parameters were a=4.1 Å and c=12.4 Å and it had superconducting properties at about T_c= 86 K.

James et al. [35], they were prepared nanoparticles of Ba_2MSnO_{6-x} (M=Ce, La and Nd) by using a polymeric combustion method. In order to get nanoparticles of these materials, scanning electron microscopy (SEM) analysis of as-prepared powders of Ba_2CeSnO_6, $Ba_2LaSnO_{5.5}$ and $Ba_2NdSnO_{5.5}$ has been used and shown that they have an average size of grains less than 50 nm. X-ray diffraction patterns of these samples were indexed; they found an ordered cubic perovskite structure. The unit cell

dimensions of the three samples are a = 8.5484 Å for Ba_2CeSnO_6, a = 8.5305 Å for $Ba_2LaSnO_{5.5}$ and a = 8.5054 Å for $Ba_2NdSnO_{5.5}$. In addition, they had double perovskite structure, with dielectric constant values are 25.67, 20.36 and 18.69, respectively, at a frequency of 107 Hz.

Firdous and Khan [36], synthesized $(Cu_{0.5}Tl_{0.5})Ba_2Ca_2Cu_{3-y}Sn_yO_{10-\delta}$ with different substituted values of (y= 0, 0.25, 0.5, 0.75, 1, 1.25, 1.5) by using solid state reaction method. The crystal structure of Sn doped samples was orthorhombic and the axis lengths were increased with enhancement of Sn concentration. The critical temperature of superconductivity was observed around 117.40, 108.41, 113.21, 98.03, 97.01, 89.21, and 85.47 K, respectively. If Sn doping concentration is enhanced beyond (y=1.5), the samples become highly resistive and have not shown any sign of superconductivity.

Irfan et al. [37], prepared the superconductor compound $Cu_{0.5}Tl_{0.5}Ba_2Ca_2Cu_2SnO_{10-\delta}$ by the solid-state reaction method, where the thallium mixed material was pressed into pellet shapes, under 0.37 GPa pressure. These pellets were enclosed in a gold capsule and heated for 10 minutes at 850°C. They measured the dc-resistivity of the samples was by four-probe method, and transition width ΔT_c of Sn doped samples was observed around 3 K. The critical temperature (T_c=99 K) and the normal resistivity (290 K) was 0.168 Ω.cm. Besids, the X-ray diffraction of this compound has shown tetragonal structure following P4/mmm space group with the (a, c) axes lengths of about 4.18 Å and 15.09 Å, respectively.

Firdoss et al [38], studied the ac susceptibility response of Sn substitution $Cu_{0.5}Tl_{0.5}Ba_2Ca_2Cu_{3-x}Sn_xO_{10-\delta}$ superconductor. The samples with maximum Sn substitution have very weak intergrain coupling and poor flux pinning as observed from their ac susceptibility measurements under the magnetic field (H_{ac}) of variable strength. They showed that H_{ac} versus T_c

curves are shifted to lower temperature with increasing Sn concentration. Their results showed that the flux pinning properties of the samples are suppressed with the increase of Sn content. It was clear the Sn concentration in CuO_2 layers not only suppresses the critical temperature but also the flux pinning strength of superconductor sample.

Mumtaz et al [39], studied the superconducting properties of $Cu_{0.5}Tl_{0.5}Ba_2Ca_2Cu_{3-y}Sn_yO_{10-\delta}$ samples, X-ray diffraction analysis of the samples under study have shown tetragonal structure following P4/mmm space group with (a, c) axes lengths of about 4.17 Å and 15.47 Å. The unit cell parameters were increased with the concentrated of Sn ratio. The dc-resistivity (ρ) versus temperature behavior of these samples have shown a metallic variation of resistivity from room temperature down to onset of superconductivity with zero resistivity at critical temperature (T_{co}) of around 100 K and The onset temperature (T_{con}) of diamagnetism were observed around 102 K.

Khan et al [40], synthesized $Cu_{0.5}Tl_{0.5}Ba_2Ca_2Cu_{3-y}Sn_yO_{10-\delta}$ by solid-state reaction; the resistivity of the samples was measured by the four probe method. The critical temperature T_c was shifted to lower temperature values with increased Sn concentration, the maximum critical temperature was about 121.1 K at y=0 and the minimum critical temperature T_c=96.5 K at y=1.5. Most of the diffraction lines of the samples without Sn concentration (prepared at 860 ^oC) were indexed as tetragonal with *P*4/*mmm* space group. However, orthorhombic distortion was produced in the Sn-substituted samples. The diffraction lines of Sn-substituted samples were fitted to the orthorhombic structure following *P*4/*mmm* space group.

Sato et al [41], synthesized a new superconductor $EuSr_2Cu_2Ta_{1-x}Sn_xO_{8-y}$ where x=0, 0.1 and 0.2 by solid state reaction. The X-ray diffraction patterns showed that the crystal structure was tetragonal of all the samples. The lattice

parameters of x=0 were a = 3.871 Å and c = 11.664 Å, and of x=0.2 were a = 3.872 Å and c = 11.674 Å. The superconducting transition temperature (T_c) was about 40 K at x = 0.2.

1.9 Literature Review of Y-family:

The superconductivity of Y-Ba-Cu-O system was discovered in 1987. The superconducting phase was identified as $YBa_2Cu_3O_{7-\delta}$ where δ=0.1. The crystal structure was determined to be orthorhombic with lattice parameters a=3.8 Å, b=3.9 Å, and c=11.7 Å [42]. This step was open the way for predication new one derived from the principle one.

Akhavan et al [43] synthesized the $Y_3Ba_5Cu_8O_{18}$ through the standard solid state reaction technique in the temperatures range 890-930 ^oC for 24 h in oxygen atmosphere. XRD patterns showed that the crystal structure of the compound was Orthorhombic phase with the lattice parameters of a=3.888 Å, b=3.823 Å, and c= 31.013 Å. The calculated values of (a, b) parameters for Y358 was very close to (a, b) parameters of Y123, but the value of c parameter of Y358 is almost 3 times more than of c-parameter for Y123. The $Y_3Ba_5Cu_8O_{18}$ compound has three CuO chains and five CuO_2 planes. The electrical resistivity indicates the transition temperature T_{co}=98 K and T_{con}=102 K.

Kruaehong et al [44], prepared the $Y_3Ba_5Cu_8O_{18}$ superconductor. They found that this compound has 2 phases, the superconductor phase and the non-superconductor phase. The resistivity measurements determined by the four probe technique had shown that T_c onset was about 94 K. The crystal structure was orthorhombic, the lattice parameters of superconducting phase were a=3.8191 Å, b=3.8867 Å, and c= 31.1662 Å, and the grain size was around 2 μm.

Udomsamuthirun et al [45] synthesized a new group of YBCO superconductors by using solid state reaction. They based on the assumption that the number of Ba-atoms plus Y-atoms is equal to the number of Cu-atoms; the resistivity measurements by the four-probe method have shown the highest T_{con} was about 94 K. The samples had shown a similar crystalline structure of Y123 and Y358 with some impurities peaks occurring by the missing of the Y-atom in some planes, and in some $Ba_2Cu_3O_5$ layers.

Vovk et al [46], investigated the conducting properties in the basal ab-plane before and after a long time exposure in air atmosphere of the optimally oxygen doped $YBa_2Cu_3O_{7-\delta}$ single crystals, that were grown in a gold crucible with the solution-melt technology. Prolonged exposure leads to an increase of the effective scattering centers of the normal carriers and to a great extent the temperature range. The normal resistivity was increased from 155 to 209 μΩ.cm, and the critical temperature dropped from 92 to 90.8 K. The width of the resistive transition to the superconducting state ΔT_c, increased approximately three fold (from 0.3 to ≈ 1 K).

Nakazato et al [47], produced bulk $YBa_2Cu_3O_y$ (Y123) superconductors with high flux pinning performance. The sample exhibited a sharp superconducting transition (around 1 K width) with an onset T_c around 93.2 K. The size of the secondary phase particles was sub-micrometer, addition to presence of small particles with a size of 100–200 nm.

Chuanbao et al [48], prepared superconductor/insulator/superconductor (SIS) junctions with $YBa_2Cu_3O_{7-x}$ films as the superconducting layers and $SrTiO_3$ as interlayer. They found that the critical transition temperatures (T_c) of the YBCO layers in the trilayer films were lower than those of the single layer YBCO films (T_c > 91 K), but the zero-resistance superconductivities of the top and bottom YBCO layers occurred at 73.2 K and 84.1 K, respectively.

Ben Salem et al [49], studied the effects of nanosized silicon oxide nanoparticles and nanowires additions on the microstructure and the normal state transport properties of polycrystalline $YBa_2Cu_3O_y$. Those were prepared by the conventional solid-state reaction method under identical conditions. The analysis of the data indicates a predominantly single phase perovskite structure Y-123 with orthorhombic *Pmmm* symmetry, and the lattice parameters were a = 0.3817 nm, b = 0.3882 nm, c = 1.1674 nm. The onset transition temperature (T_{con}) close to 93 K for all samples. The SEM results reveal that the grain size is reduced with increasing the content of SiO_2.

Guner et al [50], studied the effect of zirconium diffusion on the microstructural and superconducting properties of $YBa_2Cu_3O_{7-\delta}$ superconductors. The XRD patterns of the Zr-diffused and pure samples exhibited the polycrystalline superconducting phase with changing intensity of diffraction lines and contain the Y123 phase only. In addition to reduction of a and b lattice constants and enhancement of the unit cell parameter c, that the lattice parameters of pure Y-123 was a= 3.8286 Å, b=3.8873 Å, c=11.6938 Å. While the Zr-diffused, a=3.8202 Å, b=3.8851 Å, c=11.7224 Å. The T_{con} and T_{coff} critical temperatures were found to be about 94.4 K and 91.5 K for Zr-diffused sample as against 93.7 K and 89.4 K, respectively, for pure $YBa_2Cu_3O_{7-\delta}$. The surface of Zr-diffused sample is much smoother and denser compared to the undoped one.

Khene et al [51], prepared $YBa_2Cu_3O_{7-\delta}$ /$Y_3Fe_5O_{12}$ (YBCO/YIG) by pressing nanoparticles with high temperature sintering. The crystal structure and phase composition were characterized by X-ray diffraction (XRD) with CoK_α. The crystal structure of $YBa_2Cu_3O_{7-\delta}$ was orthorhombic structure and the unit cell parameter was a=0.38227 nm, b=0.387508 nm, and c=1.149518 nm. The onset critical temperatures for pure YBCO and YBCO+YIG 9 wt%

pellets were about of 92.37 K and 89.43 K, respectively. The grain size obtained an average of 80 nm.

Alikhanzadeh-Arani et al [52], studied influence of the utilized precursors on the morphology and properties of $YBa_2Cu_3O_{7-y}$ superconducting nanostructures. They prepared yttrium complex types by reaction of yttrium acetate with three coordination compositions, acetylacetone, 2-hydroxo-1-naphthaldehyde and salicylaldehyde. The crystalline structures of the nanoparticles remained in orthorhombic symmetry with lattice parameters a = 3.856 Å, b = 3.870 Å and c = 11.666 Å. They found that the Critical temperatures of the prepared Y123 nanoparticles were lower than that reported values of bulk Y123 material (~ 91 K). The T_c of the superconducting nanoparticles is from 82 K to 88.4 K.

Klinkova and Nikolaichik [53], studied Analytical and high resolution electron microscopic of $YBa_2Cu_3O_{7-\delta}$ samples. The samples prepared in air at 990 ^oC for 1 h then annealed in oxygen flow at 450 ^oC for 5 and 50 h. The crystal structure of Y-123 at air was tetragonal phase then transforms into the orthorhombic after oxygen annealing. Unit cell parameters of the tetragonal phase (a = 3.862 Å, c = 11.78 Å) and the orthorhombic one (a = 3.862 Å, b = 3.881 Å, c = 11.65 Å, 5 h annealing; a = 3.822 Å, b = 3.880 Å, c = 11.64 Å, 50 h annealing. The samples after 5 h oxygen annealing were having three drops at 85, 86 and 91 K. while after 50 h were having two drops at 82 and 91 K.

Zalga et al [54], prepared of $YBa_2Cu_4O_8$ (Y-124) superconductor by a sol–gel method and studied using two different complex agents with the same chemical composition. The X-ray diffraction patterns showed a single Y-124 phase. The T_c (onset) observed by resistivity and magnetic susceptibility measurements was approximately the same of the both samples (78–80 K). The SEM micrograph of the Y-124 was an average grain size of ~1–5 μm.

Giri [55], synthesized $YBa_2Cu_3O_{7-\delta}$ (YBCO) and dielectric $BaSnO_3$ samples by solid state reaction. It was observed that T_c value increases with the increase in BSO wt.%. All samples showed metallic behavior in the normal state and as superconducting transition to zero resistance. The Tc was a range (63-92) K. The pure YBCO sample exhibits large grains randomly oriented in all directions with varying size length, there is no change in grain size with the addition of BSO.

Rani et al [56], studied of $YBa_2Cu_3O_7+Ag_x$ (x=0, 0.1, 0.2), The XRD refinement for all samples were crystallized in single phase having orthorhombic structure within Pmmm space group having lattice parameter a = 3.825 Å, b = 3.889 Å and c = 11.684 Å. Relatively high normal resistivity was observed in pure YBCO than the doped samples. Also the slope of metallic resistivity was more for Ag doped YBCO than pure YBCO. All samples exhibit sharp superconducting transition with T_c ($\rho = 0$) of around 88–89 K. On the other hand, the grains of pure sample were smaller than the Ag doped sample.

1.10 The aims of research project

The aim of this research is to prepare new ceramic compounds and studying its behavior. The purpose of this selection is return to predicate the presence of new superconductor family might be appeared in those compounds. This encouraged us to select it due to the global development in high temperature superconductor compounds which proposed in international laboratories and still continuous globally. The compounds proposed are represented by $Sn_xBa_4Ca_2Cu_{x+4}O_y$ and $Y_nBa_5Cu_{n+5}O_y$ with different values of x and n, which were not proposed before comparable with the results of previous studying of Tin and Yttrium families as explained in literature review. The parameter that is dependent in this project was return to

elemental substitution in the mixture. This substitution has direct effect on the producing of new phase within the same family of superconductor compounds. The steps of this project are:

- Preparation of $Sn_xBa_4Ca_2Cu_{x+4}O_y$ with (x= 3, 4, 5, 6, 7) and $Y_nBa_5Cu_{n+5}O_y$ with (n=3, 5, 7) by the conventional method Solid State Reaction. And conclude the best value of (x, n) for both mixture respectively.
- The crystal structure and space groups lattice of the resultant of Sn-based and Y-based by using special software and databases.
- The effect of variation (x) and (n) of the compounds $Sn_xBa_4Ca_2Cu_{x+4}O_y$ and $Y_nBa_5Cu_{n+5}O_y$ on resistivity measurement, Scanning Electron Microscope and Energy Dispersive spectroscopy.

CHAPTER TWO

Experimental and Procedure

2.1 Introduction

This chapter includes the practical methods that was used to prepare and specific the superconducting state for different compounds, it is represented by the composition $Sn_xBa_4Ca_2Cu_{x+4}O_y$ with (x=3, 4, 5, 6, and 7), and the composition $Y_nBa_5Cu_{n+5}O_y$ with (n=3, 5, 7)

The experimental procedure represented by the method that was used in preparation and the techniques those were used in measurements and analysis to give a complete specification for the samples under study.

2.2 Sample Preparation of Sn-Family

The first composition ($Sn_xBa_4Ca_2Cu_{x+4}O_y$) for (x=3, 4, 5, 6, 7) has been prepared by mixing appropriate ratios of the starting materials with high purity (99.9%), SnO (Riedel Company), $BaCO_3$ (Merck Company), $CaCO_3$ (Analar Company) and CuO (Flukag Company) through the following reaction scheme:

1- For x=3

$$3SnO + 4BaCO_3 + 2CaCO_3 + 7CuO \longrightarrow Sn_3Ba_4Ca_2Cu_7O_{16} + 6CO_2$$

2- For x=4

$$4SnO + 4BaCO_3 + 2CaCO_3 + 8CuO \longrightarrow Sn_4Ba_4Ca_2Cu_8O_{18} + 6CO_2$$

3- For x=5

$$5SnO + 4BaCO_3 + 2CaCO_3 + 9CuO \longrightarrow Sn_5Ba_4Ca_2Cu_9O_{20} + 6CO_2$$

4- For x=6

$$6SnO + 4BaCO_3 + 2CaCO_3 + 10CuO \longrightarrow Sn_6Ba_4Ca_2Cu_{10}O_{22} + 6CO_2$$

5- For x=7

$$7SnO + 4BaCO_3 + 2CaCO_3 + 11CuO \longrightarrow Sn_7Ba_4Ca_2Cu_{11}O_{24} + 6CO_2$$

The procedure that was dependent to prepare SBCCO system:

1. Determine the weight of the required amounts of the starting materials by using sensitive balance with 4-digit type STATON 462AL.
2. Mixing the powder together manually by using agate mortar, the mixture then homogenized by adding a sufficient quantity of high purity 2-propanol to form a paste, during the process of remixing about 60 min, for many times.
3. Calculating the weight of the dried mixture(w1), which has grey color, and put it into alumina crucible to calcined in tube furnace in air for 24 h at 950 ^oC by programmable controller type (Eurotherm 818P). Then cooled to room temperature by the same rate. This procedure was used to remove the CO_2 from the mixture. This step should be repeated again for two or three times until the whole CO_2 removed from the mixture. When there is no further reduction in the weight, the calcination process is completed. The amount of CO_2 removed is equal to the difference in the weight before and after multi calcination process.
4. The resultant powder was grinded in agate mortar for about 30 min, to obtain very fine and optimum homogeneous powder. Then the resulting powder has been pressed into pellets in order to reduce the vacancies and porosity between the particles through the sintering process under a certain heat treatment. The dimension of the pellet was the radius of 5 mm and thickness of about 2.3 mm by using stainless steel cylindrical die. The die with diameter of 1cm that was used to prepare the pellet in a solid state laboratory. The powders were pressed using CARVAR electrical press at pressure 3 ton/cm^2. The resultant discs were subjected to sintering process under a certain heat treatment.
5. The pellets were put in an alumina crucible for sintering in tube furnace; it is process carry out at 900 ^oC for 192 hours.

During sintering the oxygen is start to flow with the certain rate 5 l/min. Sometimes the flow of Oxygen during the sintering process has direct effect in the enhancement of superconducting state during the non-stoichiometric in the elemental concentration.

The sintering process started with increasing the temperature of furnace with rate 60 ^{o}C/hr. the cooling step in the sintering process should be gradually down to 500 ^{o}C for 10 hours with a rate 30 ^{o}C/hr, then it cooled down to room temperature directly with a rate 120 ^{o}C/hr.

2.3 Preparation the composite $Y_nBa_5Cu_{n+5}O_y$

The ceramic compounds like $Y_nBa_5Cu_{n+5}O_y$ was initially obtained in the form of ceramic polycrystalline material. Appropriate weights of pure materials Y_2O_3 (Ferak Company), $BaCO_3$ (Merck Company), and CuO (Flukag Company) in proportion of their molecular weights were used in order to prepare the samples by solid state reaction. According to the following equations:

1- For n=3

$$1.5Y_2O_3 + 5BaCO_3 + 8CuO \longrightarrow Y_3Ba_5Cu_8O_{18} + 5CO_2$$

2- For n=5

$$2.5Y_2O_3 + 5BaCO_3 + 10CuO \longrightarrow Y_5Ba_5Cu_{10}O_{22.5} + 5CO_2$$

3- For n=7

$$3.5Y_2O_3 + 5BaCO_3 + 12CuO \longrightarrow Y_7Ba_5Cu_{12}O_{27.5} + 5CO_2$$

The preparation technique is done by the following steps:

1. Determine the weight of the three materials (Y_2O_3, $BaCO_3$, and CuO) by using sensitive balance with 4-digit type STATON 462AL.

2. Mixing the powders together manually by using agate mortar, the mixture become homogeneous by adding a sufficient quantity of high purity 2-propanol to form a paste, during the process of grinding for about 60 min.

3. Calculate the weight of the dried mixture, and put it in an alumina crucible calcined in tube furnace in air for 24 h at 800 ^{o}C, the calcination process carries out twice, then cooled down to room temperature by the same rate. This procedure was used to remove the CO_2 from the mixture.

4. The resultant product contained mixture with a black color. This mixture is weighed after calcination, to calculate the amount of CO_2 gas loses from it. If there is a difference in the sample weight before and after the calcinations process, is less than the theoretical value of CO_2 gas, then the calcinations process should be repeated after grinding to remove all CO_2 gas from the mixture. Then go to next step.

5. Press the powder to form a pellet shape; using CARVAR electrical press at pressure (7 ton/cm^2) then pressed the pellets of 15 mm in diameter and (1-1.5) mm thick.

6. The pellets were put in an alumina crucible for sintering in a tube furnace at temperature of 900 ^{o}C for 24 hours.

2.4 X-ray Diffraction

X-ray diffraction is one of the analytical techniques that give more information about the crystal structure, chemical composition. The crystal structures of the prepared samples were obtained by using x-ray diffraction type (PANalytical Philips) with the following features:

Source: $CuK_{\alpha 1}$

Voltage: 45 kV

Current: 10 mA

Wavelength: (1.54 Å)

The X-ray diffraction is operated by two software, the operation software and the second is analytical software (Match-2.0, X-powder and Refine95). So, the ICDD standard database of x-ray diffraction patterns enables quick phase identification for a large variety of crystalline samples.

2.5 Scanning Electron Microscope (SEM)

A scanning electron microscope (SEM) is another technique to see the morphology of sample surface. The images of a sample by scanning that is produced give more details about the grains and grains boundaries represented by the size of grain. It is also give more information about the homogeneity of grains. Sometimes, it is used to predict the nanostructure appeared in the composite prepared during the obtainable results of grain and grain boundaries. The device that was used to characterize was Inspect S 50 SEM.

2.6 Energy Dispersive Spectroscopy (EDS)

It is an analytical technique attached with SEM used for the elemental concentration analysis or chemical characterization of a sample. The electron images in the SEM display compositional contrast that the results from different atomic number elements and their distribution. Energy Dispersive Spectroscopy (EDS) allows one to identify what those particular elements and their relative proportions.

2.7 Resistivity Measurements

The most important measurement that was used to determine the type of material might be insulator, semiconductor and metal or special one the last, superconductor. It is used to measure the resistance as a function of

temperature. The electrical resistivity of the samples was measured by using the Van der Pauw method in the closed cycle Refrigerator under liquid Helium.

Van der pauw is a technique like four probe technique. The condition of the last one is the rectangular shape sample whereas in Van der Pauw used a circular shape sample. Major advantages of the new method are required a single dimension represented by the circular sample thickness, as shown in Fig. (2-1). The reason for that is return to the homogenous printed of electrodes on the sample surface which made the distance between the electrodes as proportional. According this method the resistivity of the samples can be calculated by the following equation [57]:

$$\rho = \frac{\pi\, d}{\ln 2}\, R$$

Where ρ is the resistivity, d is the thickness of the sample,

$$R = \frac{V_{CD}}{I_{AB}}$$

V_{CD} is the potential difference was measured through the points C and D.
I_{AB} is the current flow through the points A and B.

The accuracy in the R-value was investigated during the electrode replacement by V_{BC} and I_{AD}. It is necessary to record the results as the last one.

Cryostat Helium system was applied under vacuum (10^{-4} mbar). The thermometer with pt. 100 RTD thermocouple. The resistance measurement was required to connect the sample with external four points; the electrical contact had been done by using silver paste. There is a constant current path through the samples (0.05 A), the difference voltage was measured by a digital nano voltmeter type (Keithely) with sensitivity of about (± 0.1 nano volt).

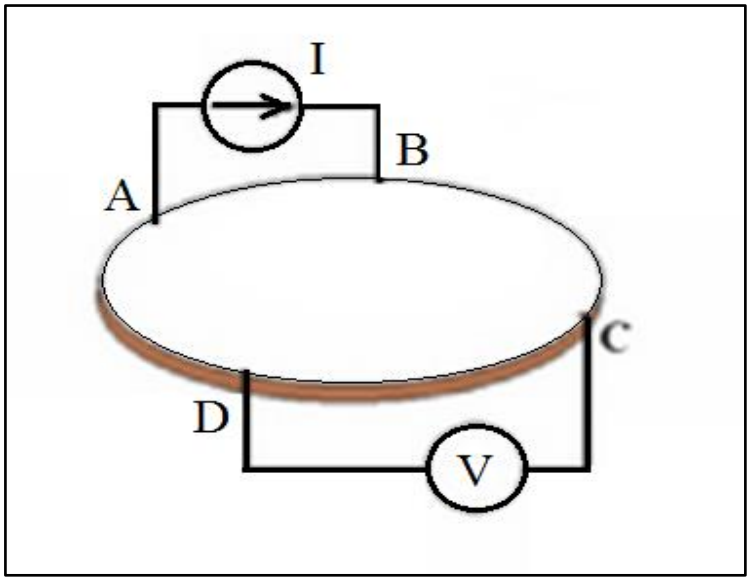

Figure 2-1: Van der pauw method to resistivity measurement.

2.8 Calculation of the critical temperature T_c

The critical temperature is the most important parameter for superconductor which being calculated by the following equation [58]:

$$T_C = \frac{T_{c1} + T_{c2}}{2}$$

Where T_c: critical temperature at the 50% of normal resistivity.

T_{c1}: temperature at the resistivity in the starting drop, 90% of normal resistivity.

T_{c2}: temperature at the resistivity approach to zero, 10% of normal resistivity.

It can determine the efficiency of the samples if it is good superconductors or not by calculating the value of ΔT_c, according to the relationship below:

$$\Delta T_C = T_c^{90\%} - T_c^{10\%}$$

Where $T_c^{90\%}$: The onset critical temperature (T_{con}) means the temperature as a function of (0.9 ρ_o).

$T_c^{10\%}$: The offset critical temperature (T_{coff}) means the temperature as a function of (0.1 ρ_o).

If the value of ΔT_c is very small in the range (1-10 K), that is favor to conclude the superconductor like type I superconductor. While if the $\Delta T_c > 10$ K, there is a vortex state superconductor. It is predication that there is a multiphase high temperature superconductor.

Furthermore; there is other critical temperature that is called the zero critical temperature that tends to make the zero resistance at a certain temperature. All the temperatures above shown in Figure (2-2).

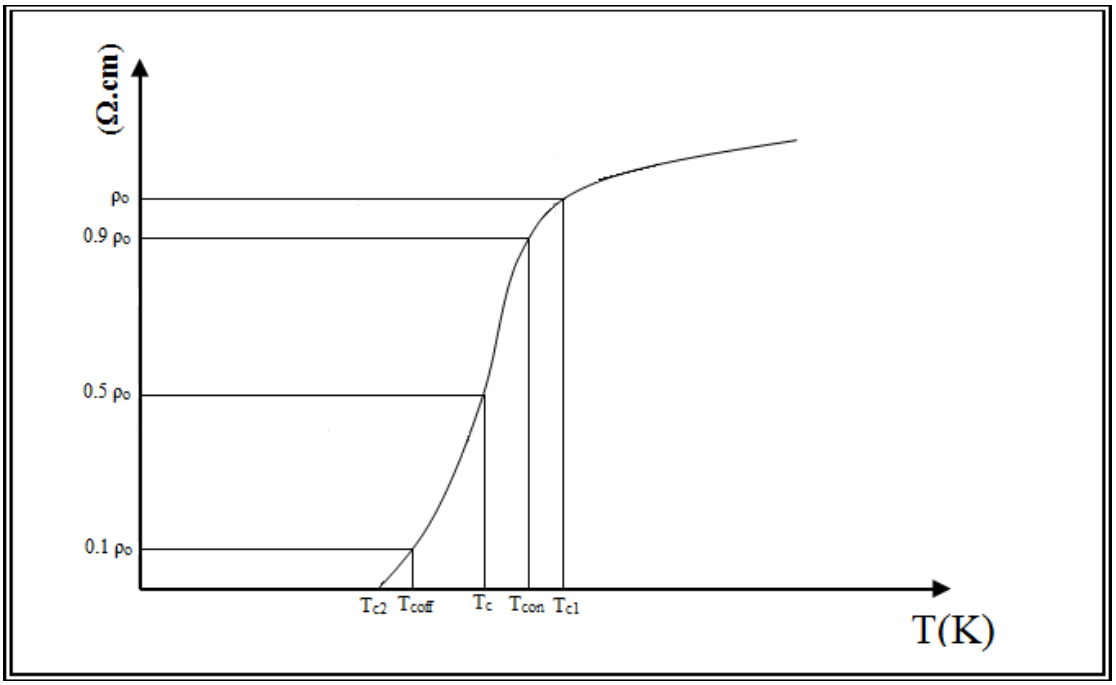

Figure (2-2): Determination of T_c and ΔT_c from the resistivity measurement.

2.9 Determination of Oxygen Content

Iodometric Titration Method is a simple chemical method [59] was used to analyses the excess in the concentration of Oxygen in the samples under study. This method carried out according to steps:

1. Weighting (40-45) mg of sample powder then grinding and placing it in a conical flask with existence the magnetic stirrer.
2. Prepare a solution of KI (2.5 ml) (3.175 g of KI with 2.5 ml of distilled water), and 1.25 ml (10%) of HCl solution then adding them together to the sample's powder, The liquid turns dark brown as I_2 is produced.
3. Adding the solution of sodium thiosulfate $Na_2S_2O_3$ (0.3 g of $Na_2S_2O_3.5H_2O$ in 20 ml of distilled water to get concentration of about (0.015 g/ml)), to the resultant liquid in previous step, by burette until the liquid becomes pale brown then adding a few drops of starch till the liquid turns dark blue.
4. Thereafter, adding of the sodium thiosulfate $Na_2S_2O_3$ solution but very slowly, stopping when the liquid becomes yellow which means the reaction is completed.
5. Measuring the volume of $Na_2S_2O_3$ solution during the total chemical reactions, which give more details about the excess of oxygen content in the mixture.

$$\delta(O_2) = \frac{\left[\frac{M_A}{M_B}\right] - \left[\frac{3m_A}{CV}\right]}{\left[\frac{2m_A}{CV}\right] - \left[\frac{M_O}{M_B}\right]}$$

Where M_A = the molar mass of the sample.

M_B = the molar mass of $Na_2S_2O_3.5H_2O$ = 248.18

m_A = weight of the sample ~ (40 - 45) mg.

M_o = the atomic weight of oxygen.

C = concentration of the $Na_2S_2O_3$ = 0.015 g/ml.

V = volume of $Na_2S_2O_3$ that used in titration.

CHAPTER THREE

Results and Discussions

3.1 Introduction

After the successful preparation of both composite families. There are many techniques and facilities, present in our laboratory, used to characterize the samples under study. There are two dependent families in this project represented by Sn-family and Y-family. The discussions of the results were involved the determination of the Oxygen excess in the mixture, structural properties, electrical properties, Scanning Electron Microscope (SEM), and Energy Dispersive Spectroscopy (EDS), give us more details about the specification of the sample under study.

3.2 Results of Iodemetric titration

As mentioned before that the effect of sintering process is tend to more dense of the sample under study during the reducing of pores size at high temperature. The second benefit is that the sample able to absorb a certain amount of oxygen content by the bombardment of oxygen flow gas on the surface of sample. The detection of this excess examined by Iodemetric titration. There is might be a partial effect on the crystal phase of sample under study. The Tin compounds showed a highest or lowest value of oxygen excess in the mixture that was depends on the insertion of Oxygen atoms within the unit cell. The results showed that (δ=0.26) per unit cell for $Sn_6Ba_4Ca_2Cu_{10}O_{22}$ and value (δ=0.1) per unit cell for $Sn_4Ba_4Ca_2Cu_8O_{18}$ there is an decreasing in the normal resistivity as a function of the excess in oxygen content, as shown in Table (3-1):

Table (3-1): The normal resistivity as a function of the excess in oxygen content.

Compounds	δ	Resistivity (MΩ.cm)
$Sn_3Ba_4Ca_2Cu_7O_{16+\delta}$	0.12	4.44
$Sn_4Ba_4Ca_2Cu_8O_{18+\delta}$	0.1	4.75
$Sn_5Ba_4Ca_2Cu_9O_{20+\delta}$	0.24	3.08
$Sn_6Ba_4Ca_2Cu_{10}O_{22+\delta}$	0.26	0.63
$Sn_7Ba_4Ca_2Cu_{11}O_{24+\delta}$	0.24	2.5

The results interpretation was related to increase the force of non-stoichiometric in the compound during the increasing of negative charge with respect to positive charge and the decreasing the normal resistivity for the system Sn-Ba-Ca-Cu-O as shown in Fig. (3-1):

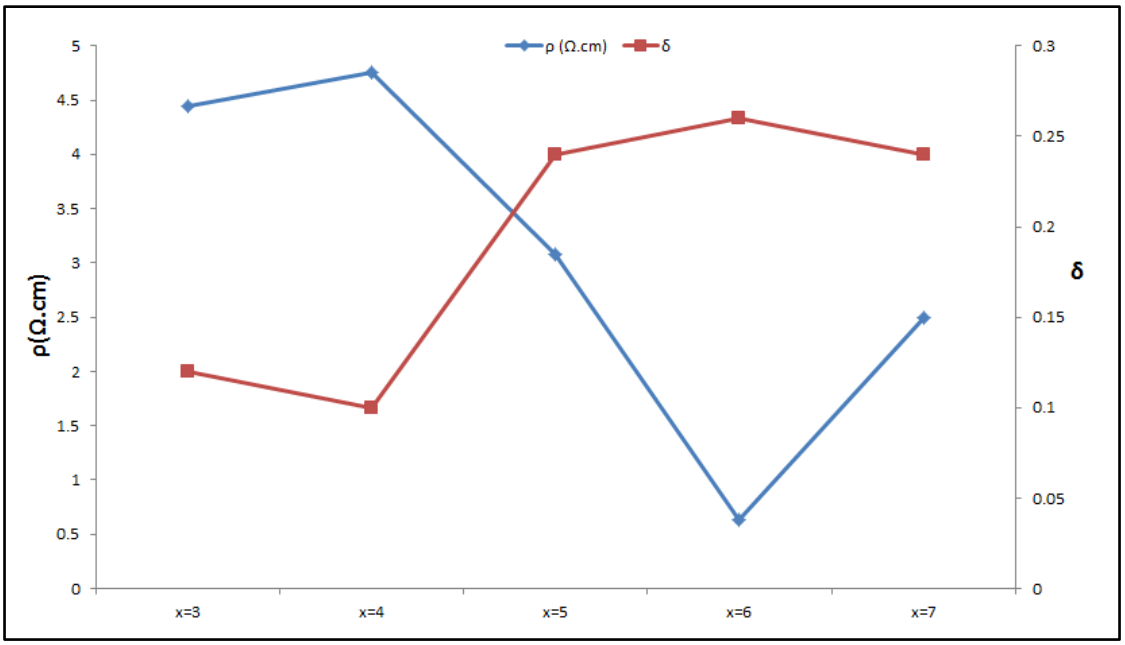

Figure (3-1): The normal resistivity and Oxygen content.

While the system Y-Ba-Cu-O prepared by solid state reaction with different composition of Y-atoms in comparable with Cu-atoms per unit cell. The amount of oxygen those were inserted in the unit cell was increased gradually with increasing the ratio of Y-atom in the compound as shown in Table (3-2). The direct increasing of normal resistivity with (δ) might be

attributed to full the vacant sites by the Oxygen atoms in the unit cell and going to saturation state. That should be increasing the scattering factor as a result of reducing the paths probability for the charge carriers to ward c-axes in the unit cell.

Table (3-2): The normal resistivity as a function of the excess in Oxygen content and critical temperature of Y-family.

Compounds	δ	Normal resistivity (mΩ.cm)	T_c (K)
$Y_3Ba_5Cu_8O_{18+\delta}$	0.18	0.035	128-113.6
$Y_5Ba_5Cu_{10}O_{22.5+\delta}$	0.21	0.796	121-113
$Y_7Ba_5Cu_{12}O_{27.5+\delta}$	0.22	14.331	128-105

3.3 XRD analysis

The XRD is an important technique to determine the structural phase represented by crystal structure, lattice parameter, and crystallite size. The prepared samples were subjected to XRD diffractometer as mentioned in chapter two. XRD software was used to determine the structural parameters of the prepared samples by using the XRD patterns which are discussed later.

3.3.1 Results of XRD for $Sn_xBa_4Ca_2Cu_{x+4}O_{2x+10}$

The XRD pattern for $Sn_xBa_4Ca_2Cu_{x+4}O_{2x+10}$ (x=3, 4, 5, 6, 7) are shown in Figures (3-2) to (3-6). There are three peaks appeared which are common peaks such as (110), (020), (123), and some time the peak (220) are common. These peaks were came from the bonds between Ba-O and Ca-O layer. The concentration of Ba and Ca will be the same for all values of x (x=3, 4, 5, 6, 7). The XRD pattern for $Sn_3Ba_4Ca_2Cu_7O_{16+\delta}$, as shown in Fig. (3-2), the highest intensity peaks were (110), (020), (123) and (220) at 2Θ (30.9, 44.1, 54.7, and 64.0) respectively, which are related to high concentration of these

planes in the structure and it is common in the appearance with all values of x. The other peaks mentioned by (016), and (033) at 2Θ (38.9, 72.63), which are low intensity, and some time are not common with other concentration of (Sn). Normally these peaks refer to Sn-O and Cu-O bonds. All these peaks were taken into account in the calculation of lattice constants. The results showed that the presence of tetragonal phase with lattice constants (a=b=4.08 Å, c=13.01 Å).

The XRD pattern for $Sn_4Ba_4Ca_2Cu_8O_{18+\delta}$ (x=4), as shown in Fig. (3-3), the most highest intensity peaks were (110), (020), (123) and (220) with 2Θ (30.7, 44.0, 54.5, and 64.0) respectively, at low intensity with respect to (x=3). That means there is a high concentration of these planes within the unit cell but lower than before. The peak (220) with 2Θ (64.0) is refer to bond from Ba-O and Ca-O, and the peak (014) refer to Cu-O bond with 2Θ=36.4. The planes (220) and (014) having lower intensity than these of x=3. The peaks (014) and (033) were shifted a slightly near its position at x=3, this change in 2Θ tend to change in the position of atoms those created these planes. There is a new creation of the peaks (101), (111) at (2Θ=22.5, 32.0) respectively with vanishing of the peak (016). There is a limited variation with respect to x=3. That is return to a slightly variation in diffraction angle of the common peaks. Secondly, the new peaks appeared and vanishing the others. The peak (101) belongs only for x=4, it might be attributed to form the bonds between the elements Sn-O. The plane (111) was created the bonds Ba-O bond. The phase was appeared as a tetragonal phase with lattice constant (a=b=4.14 Å, c=13.2 Å).

The XRD pattern for $Sn_5Ba_4Ca_2Cu_9O_{20+\delta}$ (x=5), as shown in Fig. (3-4) the most highest intensity peaks were (110), (020), (123) and (220) with 2Θ (30.5, 43.8, 54.4 and 63.8) respectively. The new peaks (005) (113) (026) were creation at 2Θ (35.4, 38.6, 61.3) but they were not common in (x=3, 4).

These peaks came from the bond of Ba-O and Ca-O. Further, the new peak (222) has 2Θ (68.0) came from the bond of Sn-O. More appearance of the Miller indices (220) which has a maximum value rather than the same peak at (x=3, 4). That means there is enhancement in the bond structure at those planes. The peak (033) common with x=3, 4 with value of 2Θ (72.4) and it showed high concentration per unit cell due to high density appeared at x=5. These were a direct effect on the limited change in the lattice constant which were (a=b=4.18 Å, c=13.38 Å) with tetragonal phase.

The common peaks are well known as mentioned before, as shown in Fig. (3-5), for x=6. There is also a common peak represented by (111) for both (x=4, 6) with the same value of 2Θ (32.0). This plane was the reason to create the Ba-O bond. The other peaks were also a copy of the last concentration at (x=5). The results showed that it has a tetragonal phase with lattice constant values a=b=4.13 Å and c=12.62 Å. This variation was related to the shifting in the diffracted peaks.

All the peaks, except the principle one (110) (020) and (123), as shown in Fig. (3-6), at x=7. These peaks are sometime a copy to the peaks for other concentration (x), others are new one. The new planes (012), (112), (007), (118), (116) were disappear from all value of (x) except x=7 due to elongation in the (b, c) axis of the structure and the peaks have 2Θ (25.2, 33.7, 51.7, 67.7, 72.8) refer to the bond between Sn-O and Cu-O. The phase calculation showed the presence of tetragonal phase with a=b=4.105 Å and c=12.2 Å. That is return to a limited variation in the position of diffracted peaks.

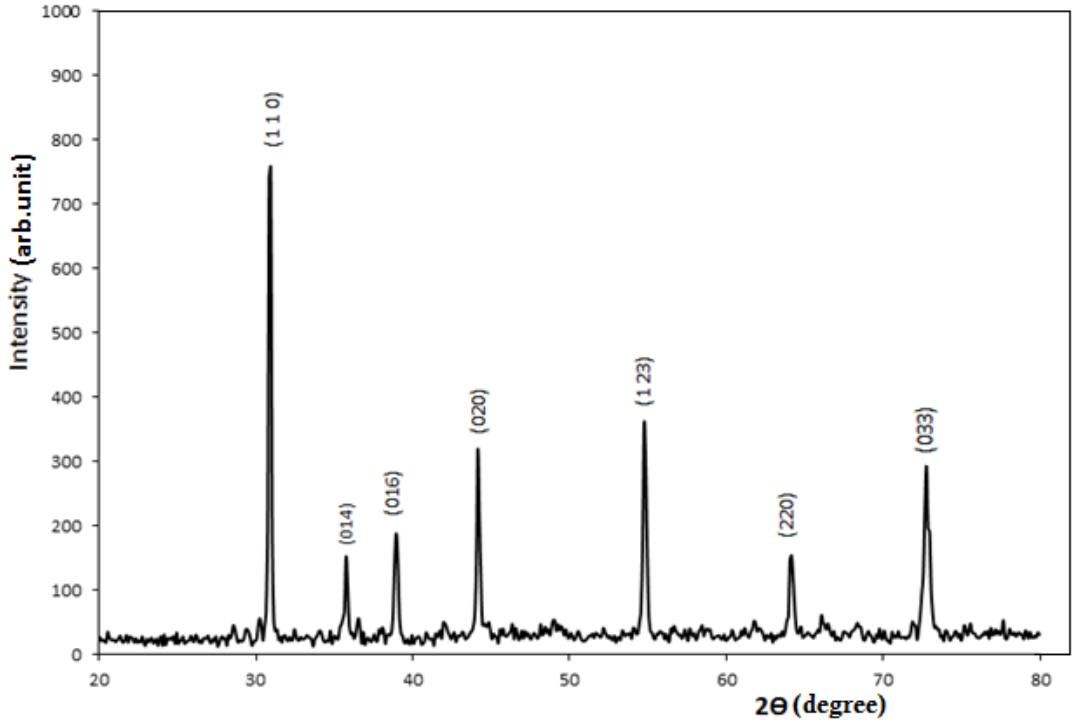

Figure (3-2): The XRD pattern for $Sn_3Ba_4Ca_2Cu_7O_{16+\delta}$

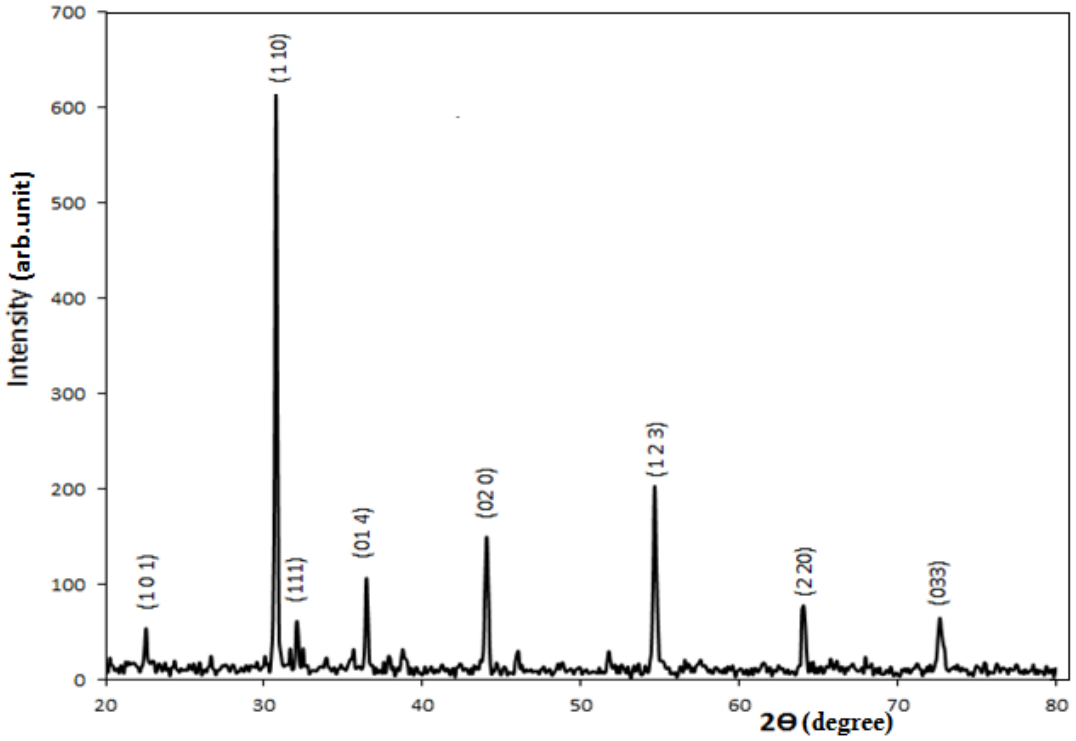

Figure (3-3): The XRD pattern for $Sn_4Ba_4Ca_2Cu_8O_{18+\delta}$

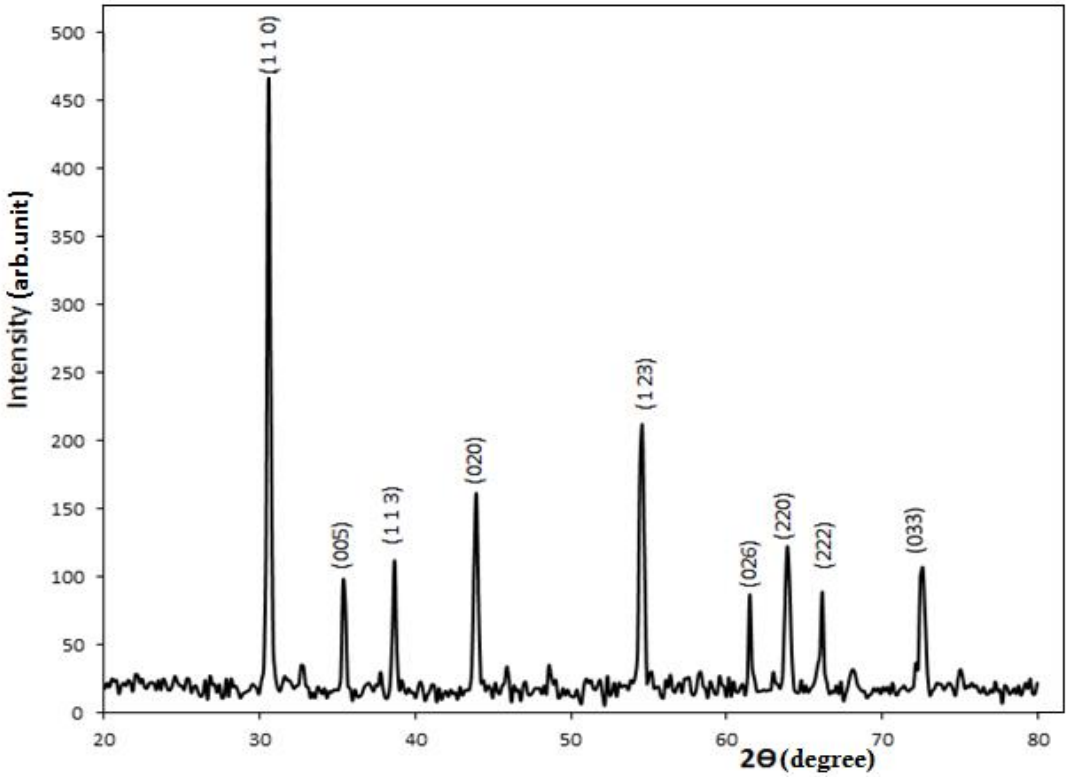

Figure (3-4): The XRD pattern for $Sn_5Ba_4Ca_2Cu_9O_{20+\delta}$

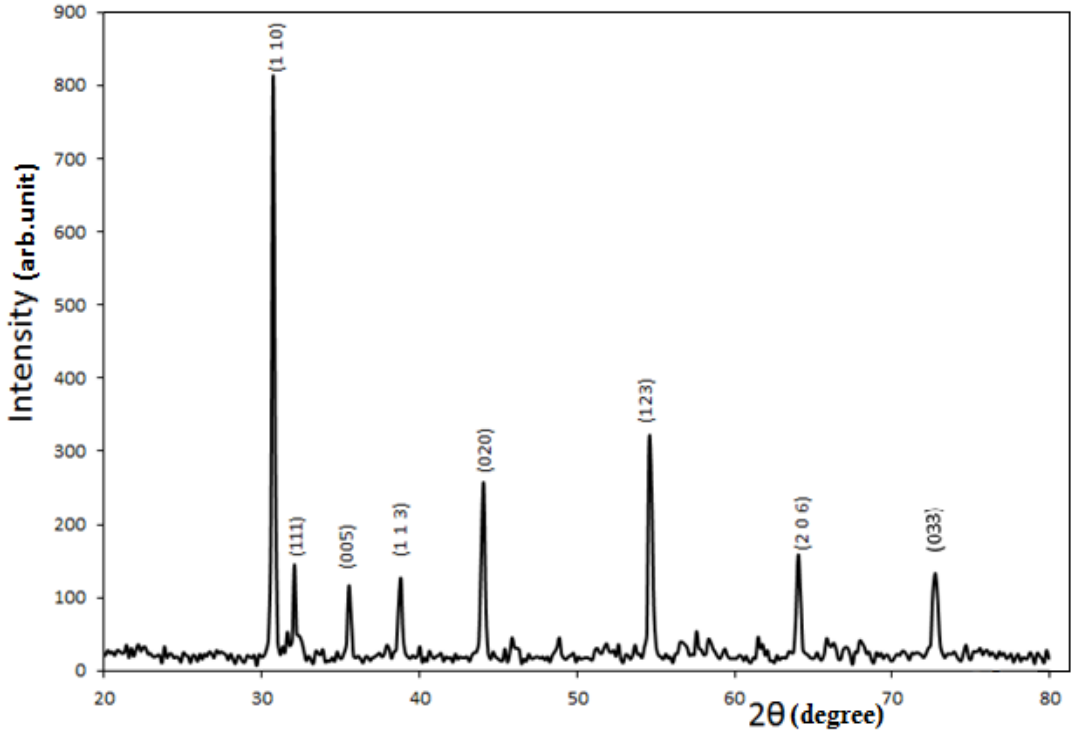

Figure (3-5): The XRD pattern for $Sn_6Ba_4Ca_2Cu_{10}O_{22+\delta}$

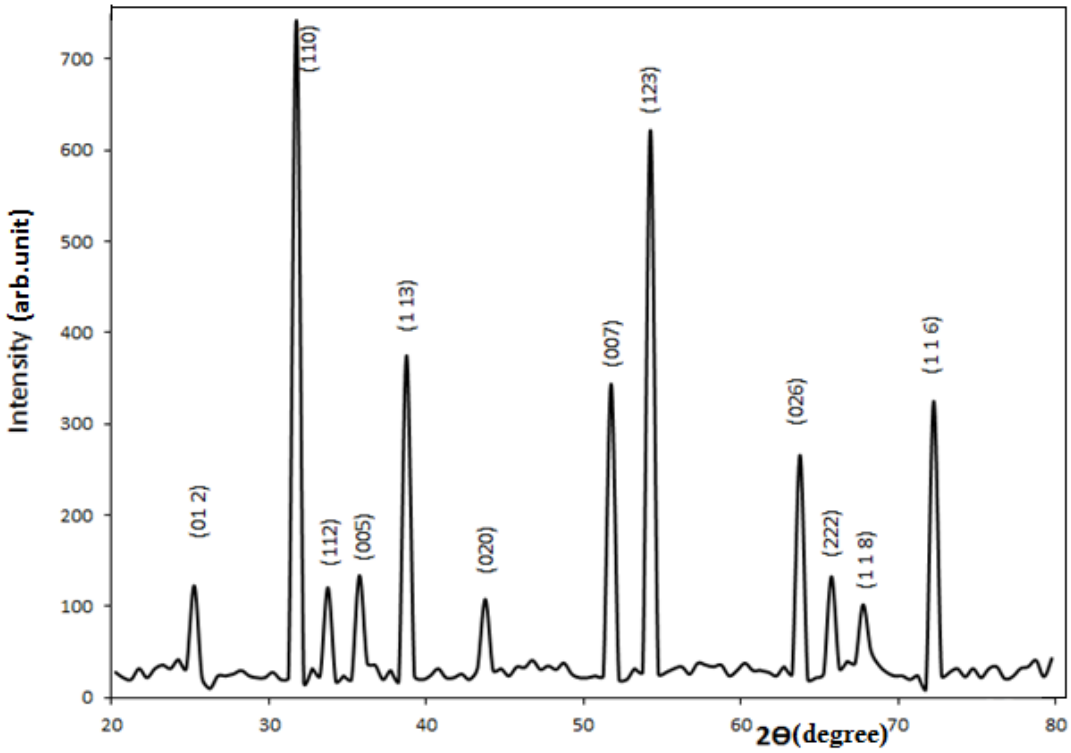

Figure (3-6): The XRD pattern for $Sn_7Ba_4Ca_2Cu_{11}O_{24+\delta}$

It was clear from the data appear in Table (3-3), there is a relationship between lattice parameters and the number of $Sn_xCu_{x+4}O_{2x+10}$ layers inserted as a function of increasing (x). The results showed at all values of x (x=3, 4, 5, 6, 7) there is tetragonal phase.

Later the extra layer of $Sn_xCu_{x+4}O_{2x+10}$ linear tend to increase a, c-axis until (x=5), that means there is elongation in a, c-axis direction as a result of extra insertion of $Cu_{x+4}O_{2x+10}$ layer within the unit cell. On the other hand, the parameters (a, c) at (x=6, 7) were goes to abrupt decreasing. That is attributed to the inversion point in the lattice parameters at x=5 within the unit cell due to the shrinkage in the basal plane. The reason for that may be attributed to the bending in the bounds with in the Basel plane. That is return to take the Oxygen atoms the interstitial site with the unit cell.

Table (3-3): Variation of a, b, c (lattice parameter), System with different values of (x) number of $Sn_xCu_{x+4}O_{2x+10}$ layers Of $Sn_xBa_4Ca_2Cu_{x+4}O_{2x+10}$

Formula	X	a (Å)	b (Å)	c (Å)	System
$Sn_3Ba_4Ca_2Cu_7O_{16+\delta}$	3	4.04	4.04	13.01	**Tetragonal**
$Sn_4Ba_4Ca_2Cu_8O_{18+\delta}$	4	4.14	4.14	13.2	**Tetragonal**
$Sn_5Ba_4Ca_2Cu_9O_{20+\delta}$	5	4.18	4.18	13.38	**Tetragonal**
$Sn_6Ba_4Ca_2Cu_{10}O_{22+\delta}$	6	4.13	4.13	12.62	**Tetragonal**
$Sn_7Ba_4Ca_2Cu_{11}O_{24+\delta}$	7	4.10	4.10	12.5	**Tetragonal**

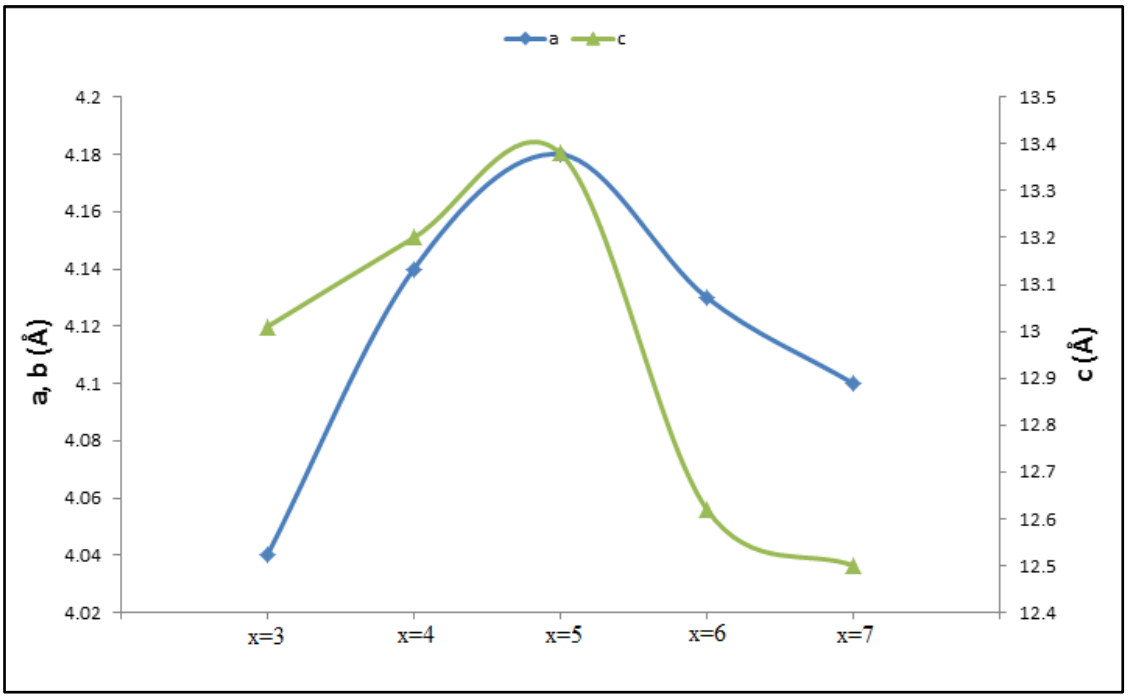

Figure (3-7): The variation of lattice constant versus the parameter (x) for $Sn_xBa_4Ca_2Cu_{x+4}O_{2x+10}$.

3.3.2 Results of XRD for $Y_nBa_5Cu_{n+5}O_y$

The XRD pattern of the samples $Y_nBa_5Cu_{n+5}O_y$ for (n=3, 5, 7) which has polycrystalline phase as shown in Figures (3-8) to (3-10). There are three common peaks appear in all phases represented by (011) (0111) (0129), which are the bases to produce the bonds between the elements Y-O and Ba-O layer. The concentration of Ba was constant within the unit cell that is

return to constant intensity of the peaks (011) for different values of (n). On the other hand, it has the same position of the diffracted angles (2θ=23.0) that means it has no effect on the partial variation of lattice constants for (n=3, 5, 7). This is a proof that the presence of Ba-atoms was strongly bonded within this plane in the unit cell. Whereas, the shifting in the diffracted angle (2θ) for the plane (0111) was appeared at (2θ=28.0, 29.9, 29.0) for (n=3, 5, 7) respectively. There is a sharp increasing in the intensity as a function of (n). That was return to increasing of Y-atom within the structure as a function of (n). This is the reason to produce Y-O bond within the planes and increasing their density as a function of (n). On the other hand, the value of (2θ= 58.95, 58.3, 58.3) for the plane (0129) at (n=3, 5, 7) respectively. The intensity of this plane was decreased as (n>3), while it remains constants at (n=5, 7). That was might be attributed to vacant position of O-site in c-axis or the chain within the unit cell. That is attributed to Y-O bond, the approaching to constant intensity of this plane give more information about the effect of increasing the density of Y-atoms within the plane (0111) rather than the plane (0129). There is agreement between the saturation of Y-atom and the saturation in oxygen excess as (n=5, 7). The slightly shifting in the diffracted angle for (n=3, 5) tend to show a decreasing in lattice constant (a) as a function of (n). This decreasing might be attributed to the bending in a-axis, but still constant at (n=5, 7) regarding to constant concentration of Y-O bond in the chain per unit cell.

The other peaks appeared in XRD patterns for the compound $Y_3Ba_5Cu_8O_{16+\delta}$ as shown in Fig. (3-8). These peaks are not common as mentioned in Fig. (3-9) and (3-10). They were mentioned by (113), (2123) have highest intensity at (2θ=33.45, 69.3), both are related to Cu-O bond. The planes were mentioned by (1018), (0119), (202) have a position (2θ=39.6,

41.15, 47.5) which were the reason to produce Cu-O bond within the unit cell of $Y_3Ba_5Cu_8O_{16+\delta}$. The position of peaks (124), (1129), (220) were at (53.35, 63.5, 75.8), those are coming from Y-O and Ba-O bonds with the unit cell. All these peaks are the property of the phase (n=3). The analytical results of XRD pattern for $Y_3Ba_5Cu_8O_y$ was exhibited Orthorhombic phase with lattice constant (a=3.852 Å, b=3.882 Å, and c=50.262 Å).

The XRD pattern for $Y_5Ba_5Cu_{10}O_{22.5+\delta}$, as shown in Fig. (3-9), it was clear that there is a major variation in the phase represented by the appearance of new peaks at (n=5, 7) in comparable with (n=3) as discussed before. The highest common three peaks were appeared (0111), (106), (0018), (111) at the position (2θ=29.9, 30.5, 31.6, 32.8). Just they were a derivative peaks from the peak (113) appeared at (n=3). The last two peaks are related to Ba-O and Y-O bonds. The peaks were mentioned with Miller indices (0026), (220) at (2θ=46.65, 68.62) respectively, they are a property of the phase (n=5). These peaks related to create Cu-O bond within the basal plane and the chain in c-axis. The results showed that there is an orthorhombic phase with the lattice constant a=3.777 Å, b=3.99 Å, c=51.93 Å. There is reduction in a-axis and increasing in b-axis with the same ratio in comparable with the composition of (n=3). These results are compatible with the results of oxygen excess within the structure, which are tend to occupy some vacant sites in the basal plane and the last made a partial variation in the dimension of ab-plane. The slightly increasing in c-axis was related to more insertion of oxygen content in the mixture.

All other peaks mentioned at (n=5) were common with the phase (n=7), except the peaks (0026), and (220) which were vanished, as shown in Fig. (3-10). On the other hand, there were a creation of new peaks appeared at (020), (2012), and (0131). This creation tend to produce a new planes inserted in the

unit cell and the last has the direct effect on the enhancement of the bonds between the elements of the structure. The important thing, there is a completely reducing of the intensity for the common peaks at (n=5, 7), that means there is a lack in the phase (n=7) in comparable with others. The peaks mentioned by (111), (0020), (1111), (1113), (1117) were the most probable peaks at (n=7) and belong to Cu-O bond. The reason for that, are approaching the quantity of oxygen excess to saturation and the last has the effect to increase the correlation between the Cu and O-atoms within the structure.

The XRD pattern of the composition $Y_7Ba_5Cu_{12}O_{27.5+\delta}$ have the most three highest intensity peaks were (0111), (106), and (111), and the lower intensity were mentioned by the peaks (0018), (020), (2012), (0131) at the position (2θ=31.6, 46.66, 52.4, 61.4), these planes may be attributed to form Cu-O bonds. The analytical results of XRD pattern for $Y_7Ba_5Cu_{12}O_{27.5+\delta}$ was exhibited orthorhombic phase with lattice constant (a=3.62 Å, b=4.01 Å, c=52.31 Å). There is a slightly variation of lattice constants in comparable with others, that is related to slightly variation in the position of diffracted angles, secondly there is vanishing and creation in some peaks appeared.

Actually the changes in the unit cell structure are a function of (n), the last are the reason to create or diminish the planes within the structure. There is more reduction in a-axis of the unit cell and slightly increasing in the b-axis. This variation is proportional to different values of (n=3, 5, 7). That is related to more dense of Y-atom within the unit cell, which was the reason to more insertion of O-atom within the unit cell especially in the basal plane. In the same time, there is increasing in the c-axis regarding to this conditions. The lattice parameter variation as a function of Y-atom concentration and Cu-O layer inserted in the structure, which are the reason to presence the defect concentration and producing the nonstoichiometric composition. That is

might be attributed to the shrinkage in the basal plane with the unit cell. The interpretation for that is the reduction of the vacancies or oxygen sites in the basal plane, which was confirmed with the $T_{c,}$ concluded. The CuO_2 layers inserted as a function of increasing (n), it was well defined with increasing Y-atom concentration and the number of CuO_2 layer led to linear increasing in b and c-axis [43], and the c-axis was increased five time of Y123, in contradiction with previous studies [60,61]. On other hand, the parameter (a) showed a slightly decreasing keeping the orthorhombic is still present, as shown in Table (3-4).

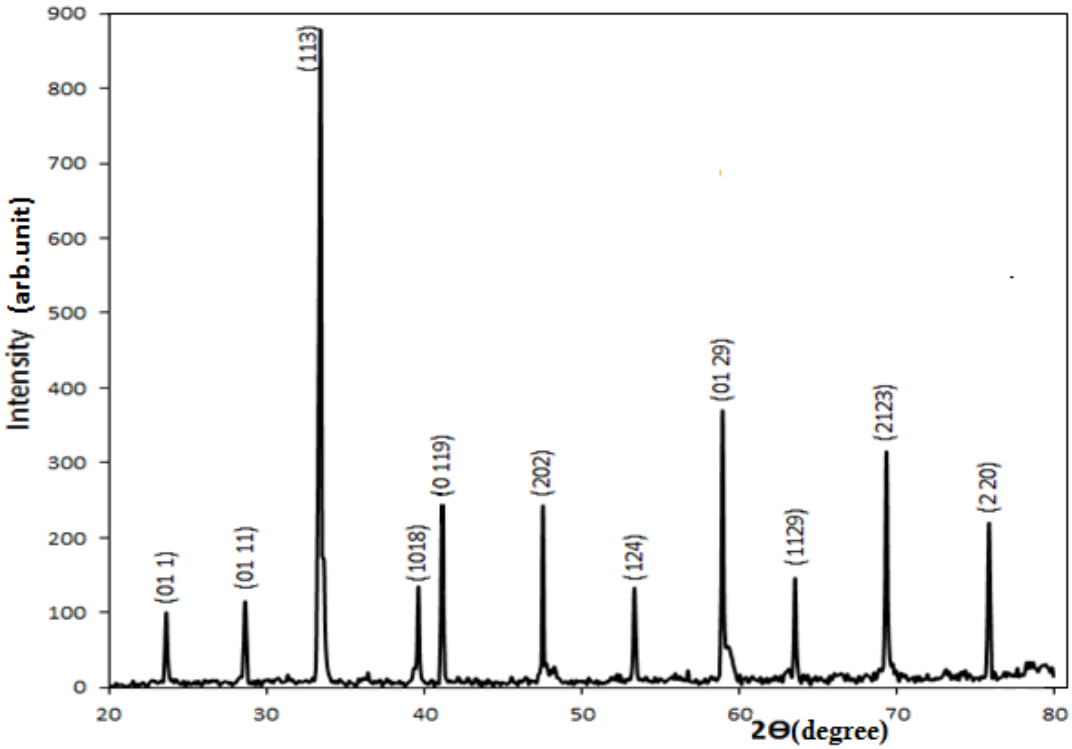

Figure (3-8): The XRD pattern for $Y_3Ba_5Cu_8O_{16+\delta}$

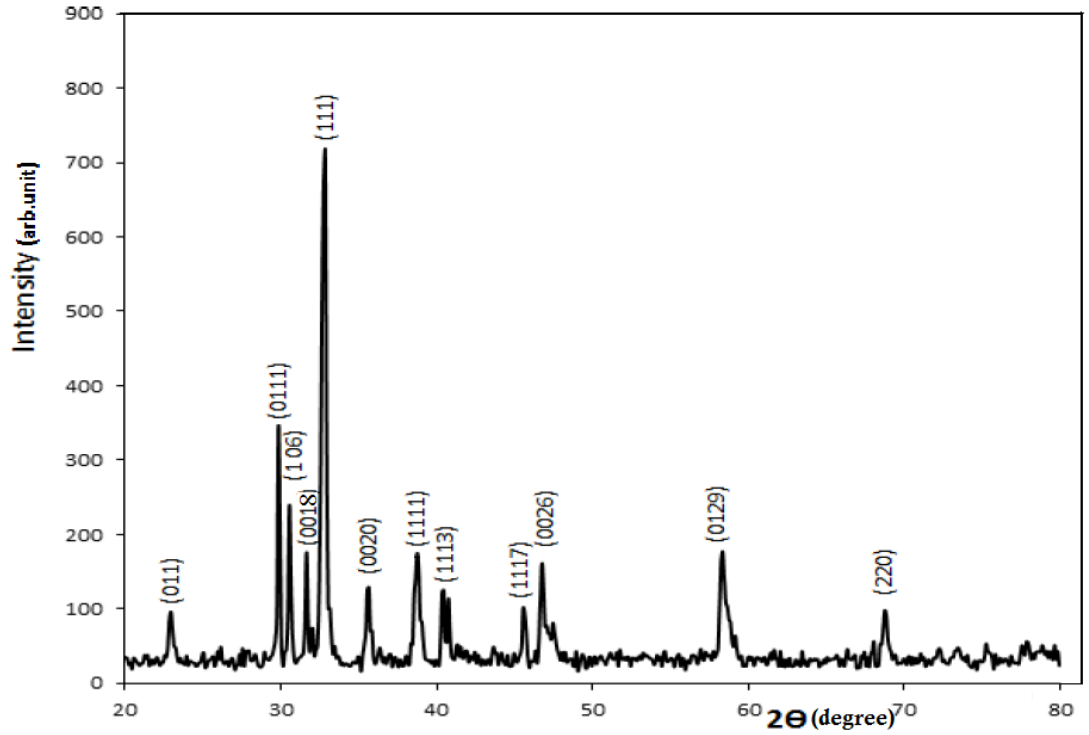

Figure (3-9): The XRD pattern for $Y_5Ba_5Cu_{10}O_{22.5+\delta}$

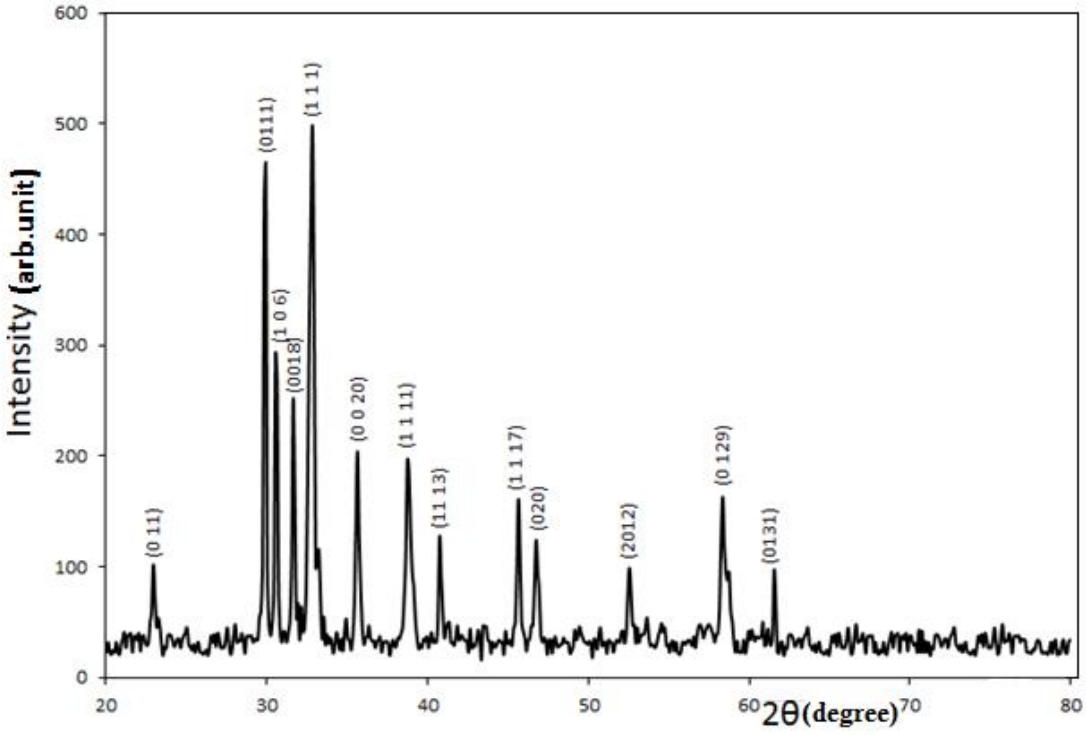

Figure (3-10): The XRD pattern for $Y_7Ba_5Cu_{12}O_{27.5+\delta}$

Table (3-4): Variation of a, b, c (lattice parameter), System with different values of (n) number of CuO_2 layer Of $Y_nBa_5Cu_{n+5}O_y$

Formula	n	a (Å)	b (Å)	c (Å)	System
$Y_3Ba_5Cu_8O_{18+\delta}$	3	3.852	3.882	50.262	**Orthorhombic**
$Y_5Ba_5Cu_{10}O_{22.5+\delta}$	5	3.777	3.99	51.93	**Orthorhombic**
$Y_7Ba_5Cu_{12}O_{27.5+\delta}$	7	3.62	4.01	52.31	**Orthorhombic**

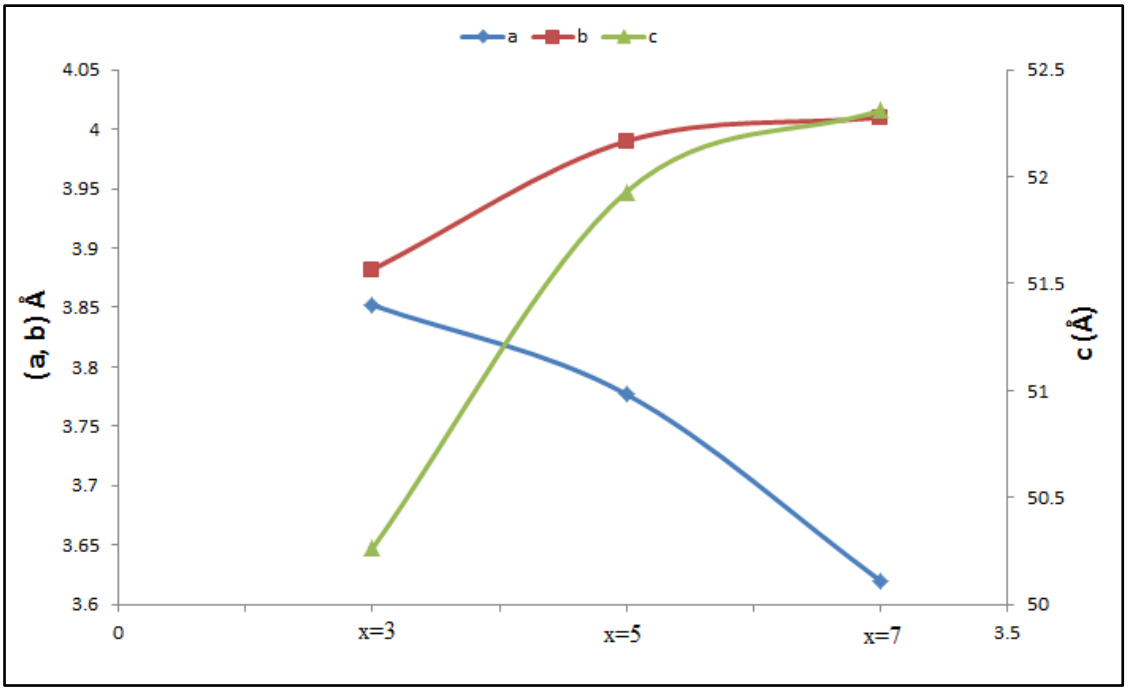

Figure (3-11): The variation of lattice constant versus the parameter (n) for $Y_nBa_5Cu_{n+5}O_y$.

3.4 Results of Electrical Resistivity

The temperature dependence of resistivity for all samples under study was measured by using Van der pauw technique. The closed cycle refrigerator under liquid helium was used with controllable heat temperature to perform the resistivity measurements especially at low temperature as mentioned before in chapter two. The resistivity results of Sn-family showed the general behavior represented by increasing of resistivity with decreasing temperature to ward low temperature of about (110 K) as shown in Figures (3-12) and (3-

13). That is attributed to semiconducting behavior of the samples prepared by Sn-Ba-Ca-Cu-O. The activation energy of all compounds of Sn and the energy gap shown in Table (3-5):

Table (3-5): The activation energy and energy gap of Sn-family.

The compounds	The activation energy (e.v)	Energy gap (e.v)
$Sn_3Ba_4Ca_2Cu_7O_{16+\delta}$	0.0304 – 0.039 – 0.0195	0.078
$Sn_4Ba_4Ca_2Cu_8O_{18+\delta}$	0.131 – 0.0465 – 0.0112	0.262
$Sn_5Ba_4Ca_2Cu_9O_{20+\delta}$	0.0681 – 0.0476 – 0.011	0.136
$Sn_6Ba_4Ca_2Cu_{10}O_{22+\delta}$	0.1271 – 0.0837	0.254
$Sn_7Ba_4Ca_2Cu_{11}O_{24+\delta}$	0.1251 – 0.035 – 0.0236	0.25

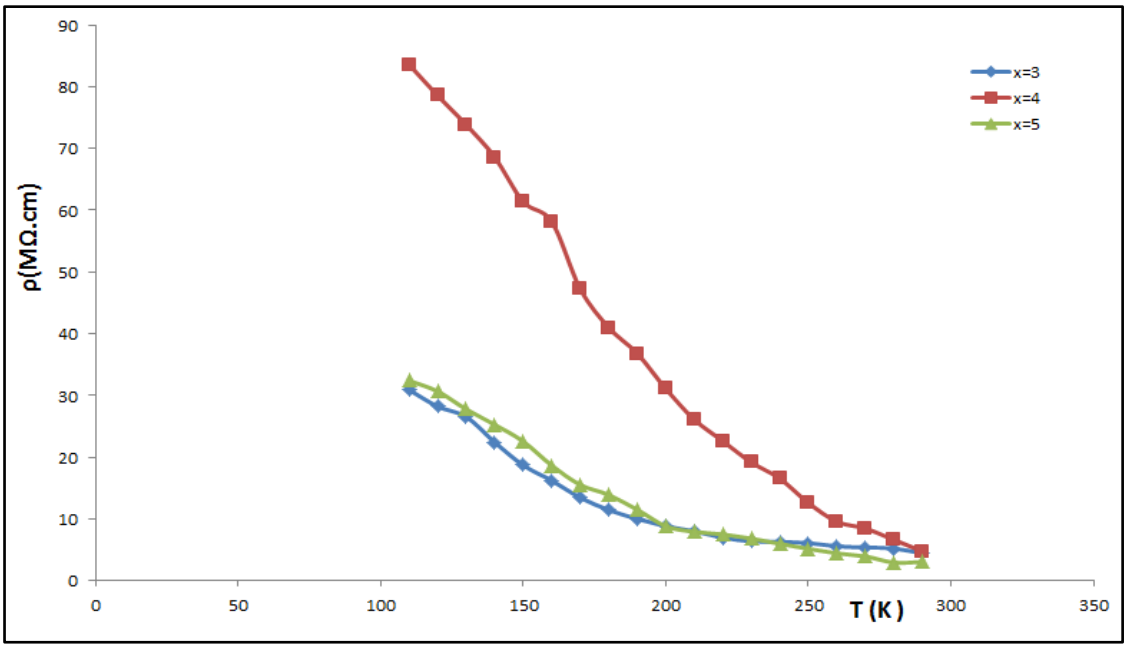

Figure (3-12): The resistance as a function of temperature for Sn-family (X=3, 4 and 5)

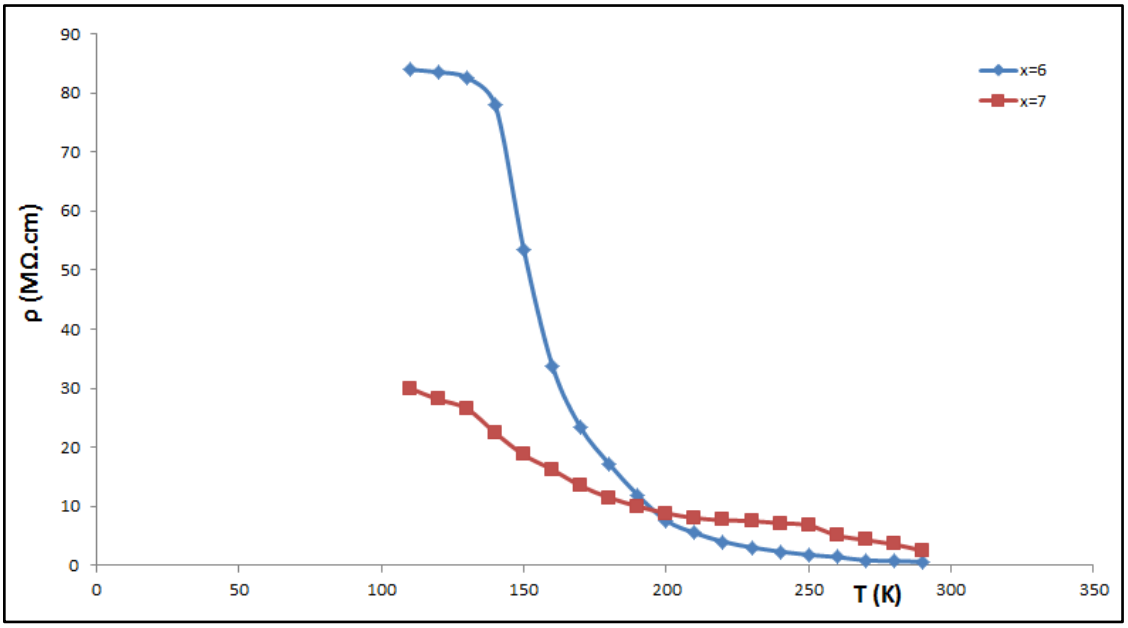

Figure (3-13): The resistance as a function of temperature for Sn-family (X=6, 7).

The results of resistivity for the system Y-Ba-Cu-O by using the same procedure discussed before. In general the compounds of the system Y-Ba-Cu-O showed a superconductor behavior and good results in the resistivity behavior.

The sample $Y_3Ba_5Cu_8O_{18+\delta}$ that was sintered at (900 ^oC) for (48 hr) has two steps in the resistivity behavior, as shown in Fig. (3-14), in contradiction with previous studies [43, 44], they found a single phase of Y358. The first step was in the temperature range (T= 260-125 K) and the second step was in the range (T= 125-110 K). That is related to presence of multi-phase superconductor with polycrystalline structure as mentioned before in X-ray diffraction results. There are two critical temperature was about (T_{c1}= 128 K) and (T_{c2}= 113.6 K), so it was concluded that there is a vortex state within the temperature range (T_c=128-113.6 K) that was clear from the multiphase appeared as mentioned before. The value of (ΔT_c) was measured, it was (ΔT_{c1}=10 K) for the first step and (ΔT_{c2}=1.3 K) for the second one. The presence of superconducting domain in a vortex state is considering the key to

distribute these domains near the surface for the first step and others in the center of the sample. This is the reason why the presence two different values of (ΔT_c) with different temperature range. It is well define that the penetration depth has a direct effect on the distribution of these domains, so it was preferable the compatible between the long range of (ΔT_{c1}) and the penetration depth.

The resistivity measurement for the sample $Y_5Ba_5Cu_{10}O_{22.5+\delta}$ was shown in Fig. (3-15), it was exhibited that there is also two variable regions. The first region appeared in the temperature range (T= 250-120 K) and the second was appeared in the temperature range (T= 120-110 K). The abrupt variation of resistivity curve near T_c-value is well defined in comparable with previous one. There is a vortex state represented by the presence of two values of (T_{c1}= 121 K) for the first region and (T_{c2}= 113 K) for the second region. There is equal limited values of (ΔT_c) represented by (ΔT_{c1}= 2.5 K) for the region one and (ΔT_{c2}= 1.5 K) for the region two. That is making to predicate that the distribution of vortex domains is symmetric for the all sample under study regarding to the approaching in ΔT_c-values, which was agreed with the result of X-ray that was discussed before.

On the other hand, the compound $Y_7Ba_5Cu_{12}O_{27.5+\delta}$ that has vortex state also and producing two T_c-value represented by (T_{c1}= 128 K) within the temperature range region (T= 250-125 K) and (T_{c2}= 105 K) with the temperature range region (T= 125-103 K). The values of (ΔT_{c1}= 2 K) and (ΔT_{c2}= 1.3 K) for first and second step respectively are shown in Fig. 6. The approaching in ΔT_c-values tends to conclude the distribution of all superconducting domains is the same along all sample dimensions. The similarity in the results appeared in Figures (3-15) and (3-16) made the predication of the unique in the phase is acceptable more than the results

appeared in Fig. (3-14). The thing is supporting this conclusion was clear for undefined peaks in the phase (n=3) rather than the phases (n=5, 7).

The normal resistivity for $Y_3Ba_5Cu_8O_{18+\delta}$, $Y_5Ba_5Cu_{10}O_{22.5+\delta}$ and $Y_7Ba_5Cu_{12}O_{27.5+\delta}$ was exhibited different values, which were (0.035 mΩ.cm), (0.79 mΩ.cm) and (14.33 mΩ.cm) respectively. It was clear that there is a sharp increasing in the resistivity with increasing n-value. It is well defining the mechanism of conductivity toward the c-axis, the results showed increasing in the c-axis and the last has the direct effect on the motion free electron and in the same time increasing the scattering factor for these electrons above T_c. This is the main reason for increasing the resistivity with increasing the ratio of Y-atoms in the mixture.

The overall conclusions showed that there is a superconductor behavior but different value of T_c to ward of decreasing in (T_c) value with increasing of Y-atoms concentration in the mixture. There is a harmony in the distribution of positive ions within the unit cell in comparable with negative ions, which were agreed with previous study [43, 44]. The electrical resistivity indicates the transition temperature for $Y_3Ba_5Cu_8O_{18}$ was T_{c0}= 98 K and T_{con}=102 K, these result was by Akhavan [43].

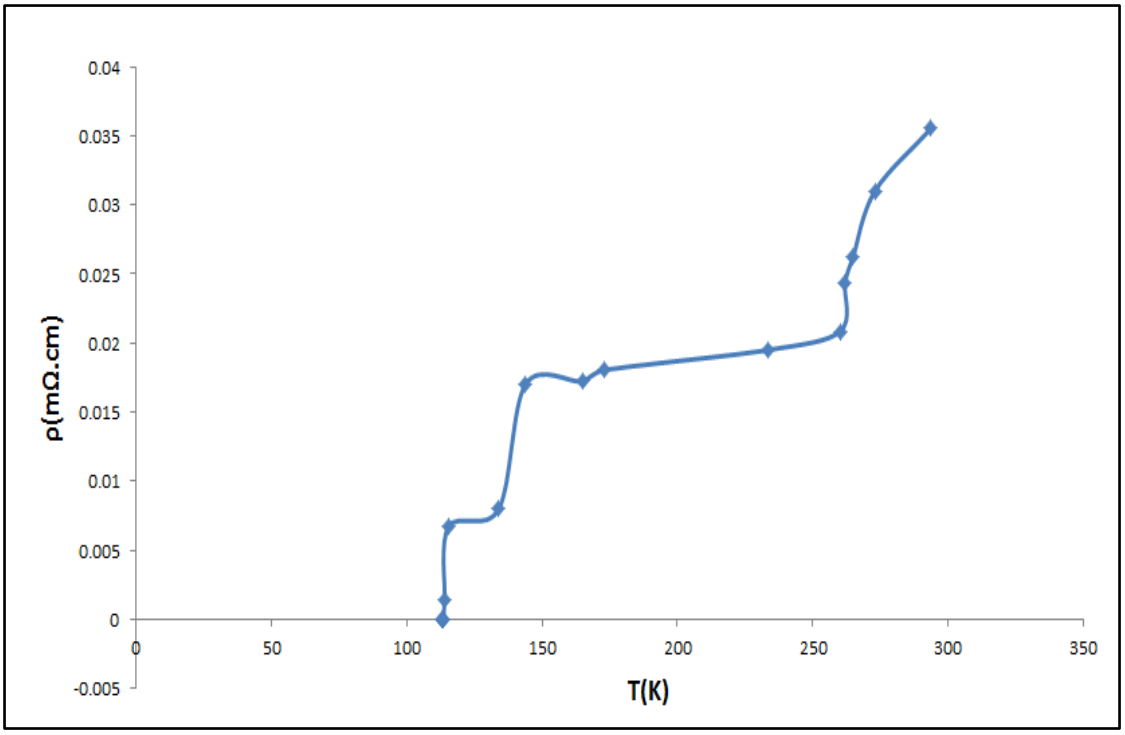

Figure (3-14): The resistance as a function of temperature for $Y_3Ba_5Cu_8O_{18+\delta}$.

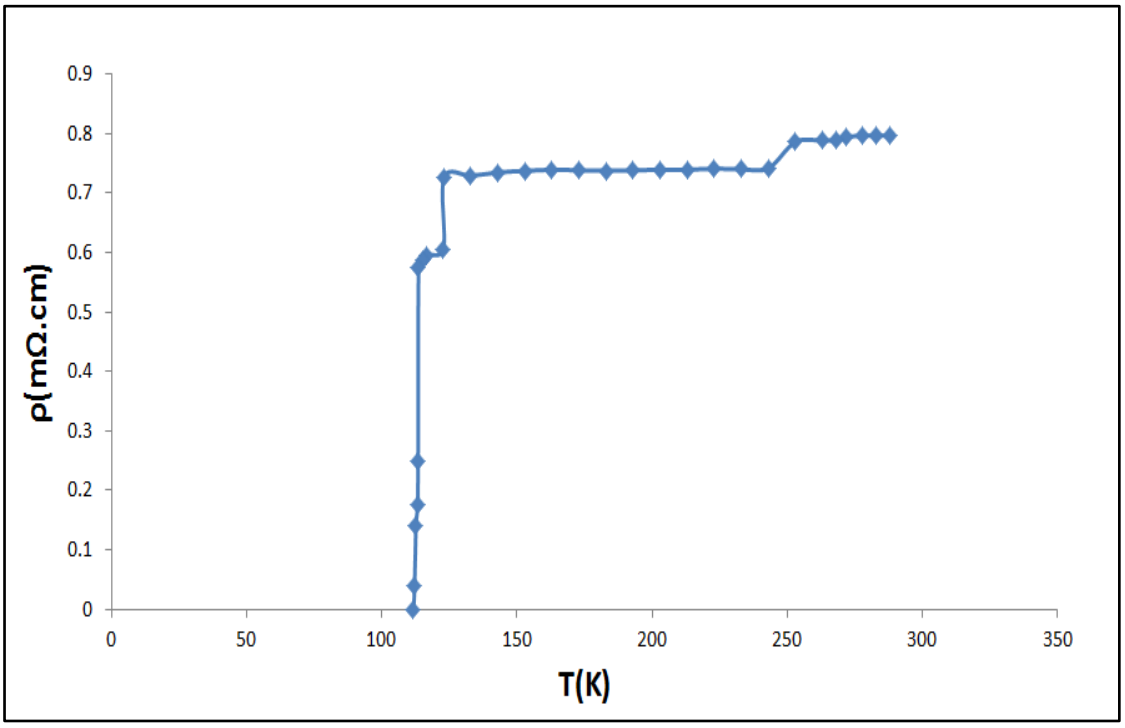

Figure (3-15): The resistance as a function of temperature for $Y_5Ba_5Cu_{10}O_{22.5+\delta}$.

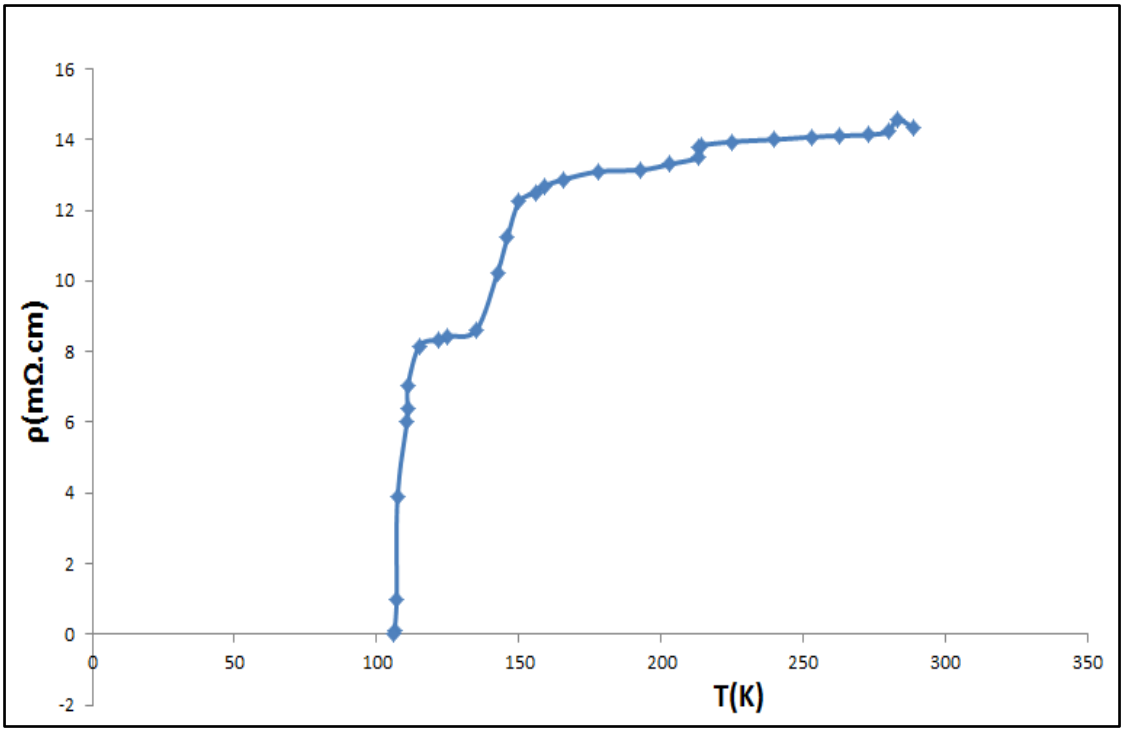

Figure (3-16): The resistance as a function of temperature for $Y_7Ba_5Cu_{12}O_{27.5+\delta}$.

3.5 Results of SEM

The Scanning Electron Microscopy (SEM) is another technique used to complete the specification for the samples under study. The high resolution images of surface morphology produced tend to know the nature of grain and porous size. In addition to that, it is used to give us more details about the homogeneity of the powder produced by high magnification process in comparable with optical microscope.

Qualitative and quantitative chemical analysis information is also obtained by using energy dispersive X-ray spectrometer (EDS) which is a complement with SEM.

The image of the samples $Sn_3Ba_4Ca_2Cu_7O_{16+\delta}$ and $Sn_5Ba_4Ca_2Cu_9O_{20+\delta}$ showed there is no homogeneity for the sample under study as exhibited Fig. (3-17). That was appeared by the shape of grains and their size. The range of grain size was about (1-5 μm). There is a type of merging shape in such points. While in $Sn_4Ba_4Ca_2Cu_8O_{18+\delta}$ showed homogeneous

granules with clear boundaries, the range of grain size was about (0.7-3 µm). While in the $Sn_6Ba_4Ca_2Cu_{10}O_{22+\delta}$ and $Sn_7Ba_4Ca_2Cu_{11}O_{24+\delta}$ the starting of nanostructure in the samples were created represented by nano road. Their diameter in the range (100-300 nm).

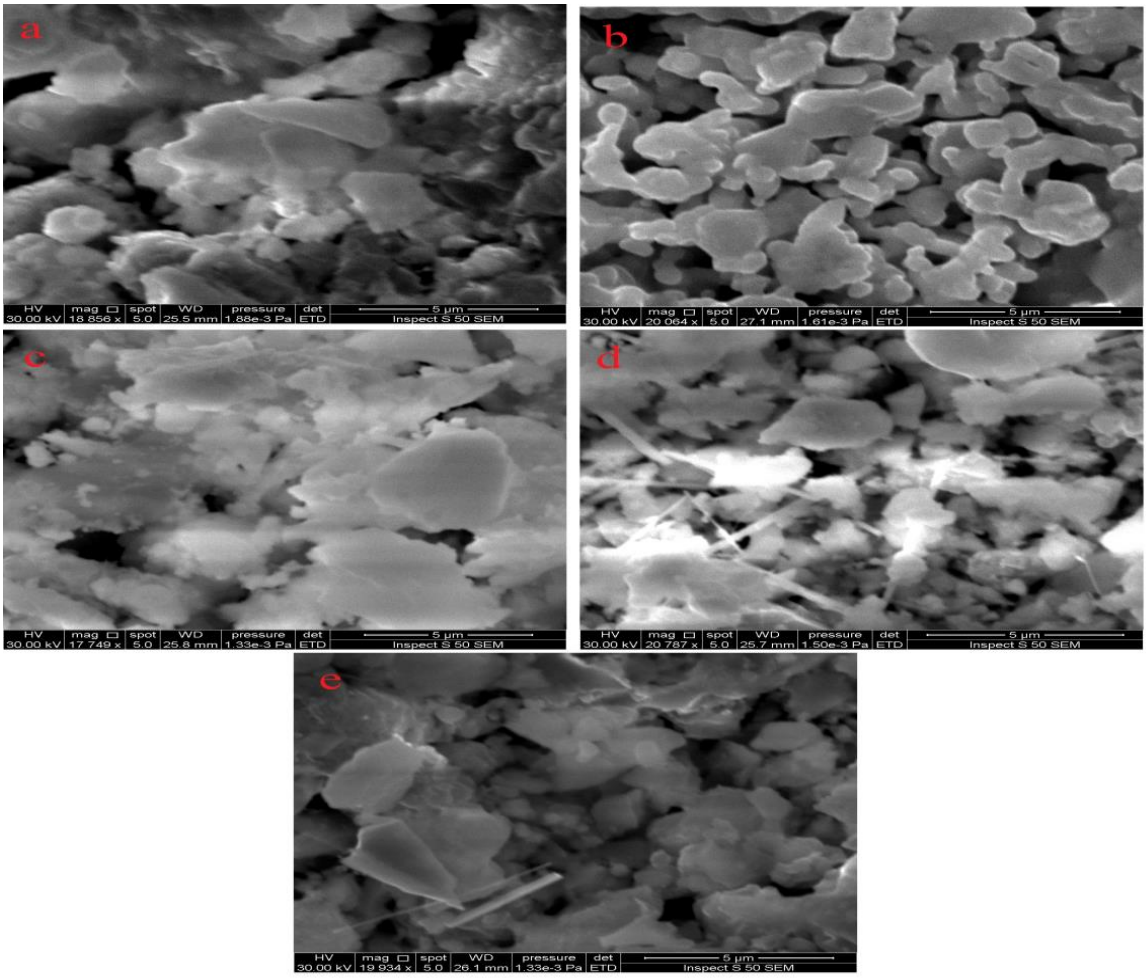

Figure (3-17): SEM micrographs of Sn-family. (a) $Sn_3Ba_4Ca_2Cu_7O_{16+\delta}$ (b) $Sn_4Ba_4Ca_2Cu_8O_{18+\delta}$ (c) $Sn_5Ba_4Ca_2Cu_9O_{20+\delta}$ (d) $Sn_6Ba_4Ca_2Cu_{10}O_{22+\delta}$ (e) $Sn_7Ba_4Ca_2Cu_{11}O_{24+\delta}$.

Fig. (3-18) shows SEM micrographs of pure YBCO samples, the $Y_3Ba_5Cu_8O_{18}$ exhibits large grains randomly with size varying from 1 to 6 µm as shown in Fig. (3-18a). While $Y_5Ba_5Cu_{10}O_{22.5+\delta}$ and $Y_7Ba_5Cu_{12}O_{27.5+\delta}$ have grains appeared to be clear and the range in size between (700 nm-4 µm). In addition to the emergence of interfaces distances that were not present in the

$Y_3Ba_5Cu_8O_{18+\delta}$ sample. The engineering of fine Y_2BaCuO_5 (Y-211) inclusions of average particle size (1-2 μm), these result conclude by Thoma et al [62]. Whereas Alecu [63], found that the grain size of $YBa_2Cu_3O_{7-\delta}$ superconductor increased (~ 10 μm).

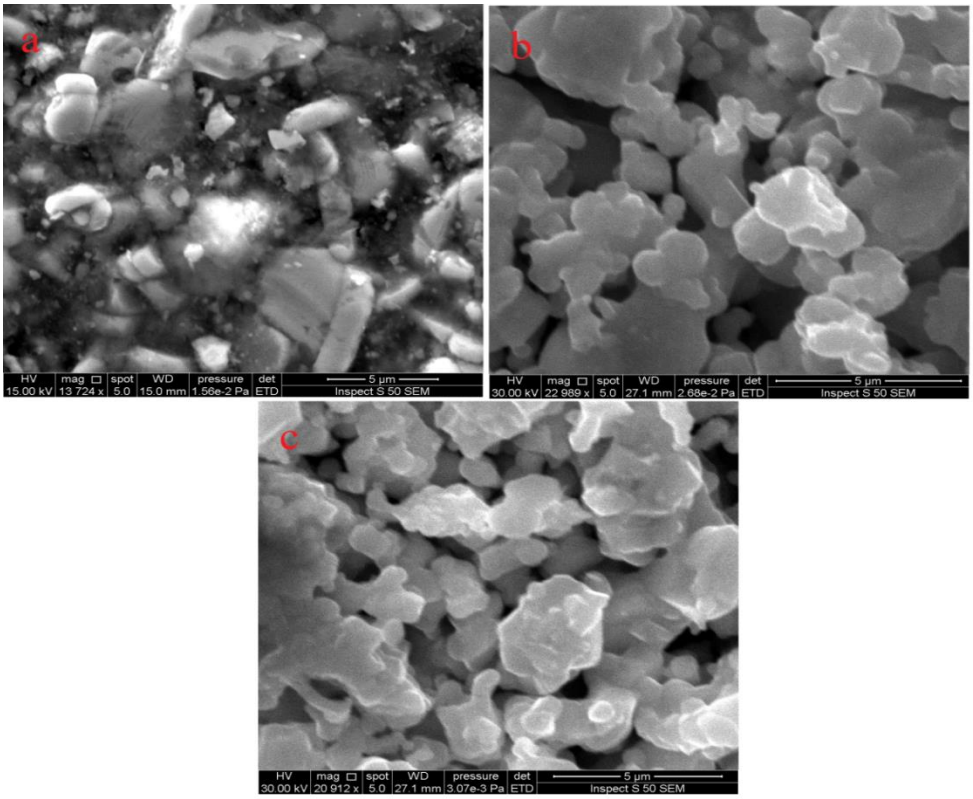

Figure (3-18): SEM micrographs of Y-family. (a) $Y_3Ba_5Cu_8O_{18+\delta}$ (b) $Y_5Ba_5Cu_{10}O_{22.5+\delta}$ (c) $Y_7Ba_5Cu_{12}O_{27.5+\delta}$.

3.6 Results of EDS

The analysis of EDS which is a complement with SEM was considering the tools to find the percentage ratio of the elements in the mixture. The aim of this analysis is to satisfy the theoretical ratio with experimental one. In general the compounds $Sn_xBa_4Ca_2Cu_{x+4}O_y$ with different value of (x=3, 4, 5, 6 and 7) showed all the elemental ratios represented by the Figures (3-19) to (3-23) respectively. The peaks mentioned are related to the energy of each

element in the mixture. On the other hand it is clear that the intensity of each peak is regarding to the percentage ratio of each elements in the compound.

The main conclusions of EDS are regarding to the concentration of charges for Sn compounds and satisfy the ratio of cation to anion in the mixture. The last one has a direct effect on the behavior of resistivity with temperature for both families of compounds. The compounds of Y-Ba-Cu-O as explained in Figures (3-24) to (3-26) showed also the presence of basic elements which have proportional approach to theoretical values derived from chemical equation.

The results showed that the agreement of the peaks appeared with the theoretical values. In addition to that, the results of Y-Ba-Cu-O system exhibited more satisfaction with the theoretical one.

That is return to the coincidence of charges concentration represented by anion to cation with results of resistivity appeared previously, which were exhibited very low normal resistivity in comparable with the compounds of the system Sn-Ba-Ca-Cu-O.

Tables (3-6) to (3-9) have shown the experimental and the theoretical results of Sn-Ba-Ca-Cu-O and Y-Ba-Cu-O systems.

Table (3-6): Theoretical concentration of elements in compound $Sn_xBa_4Ca_2Cu_{x+4}O_{2x+10}$

X	Sn %	Ba %	Ca %	Cu %	O %
3	9.37	12.5	6.25	21.87	50
4	11.11	11.11	5.55	22.22	50
5	12.5	10	5	22.5	50
6	13.63	9.09	4.54	22.72	50
7	14.58	8.33	4.16	22.91	50

Table (3-7): Experimental concentration of elements in compound $Sn_xBa_4Ca_2Cu_{x+4}O_{2x+10+\delta}$

X	Sn %	Ba %	Ca %	Cu %	O+δ %
3	8.96	12.25	5.93	21.62	51.24
4	10.95	10.84	5.13	21.89	51.19
5	12.25	9.62	4.34	22.13	51.66
6	13.04	8.53	4.05	22.28	52.1
7	14.23	7.81	3.67	22.64	51.67

Table (3-8): Theoretical concentration of elements in compound $Y_nBa_5Cu_{n+5}O_y$.

n	Y %	Ba %	Cu %	O %
3	8.82	14.7	23.52	52.94
5	11.76	11.76	23.52	52.94
7	13.59	9.7	23.3	53.39

Table (3-9): Experimental concentration of elements in compound $Y_nBa_5Cu_{n+5}O_{y+\delta}$.

n	Y %	Ba %	Cu %	O+δ %
3	8.52	14.52	23.22	53.74
5	11.43	11.36	23.25	53.96
7	13.26	9.35	22.95	54.44

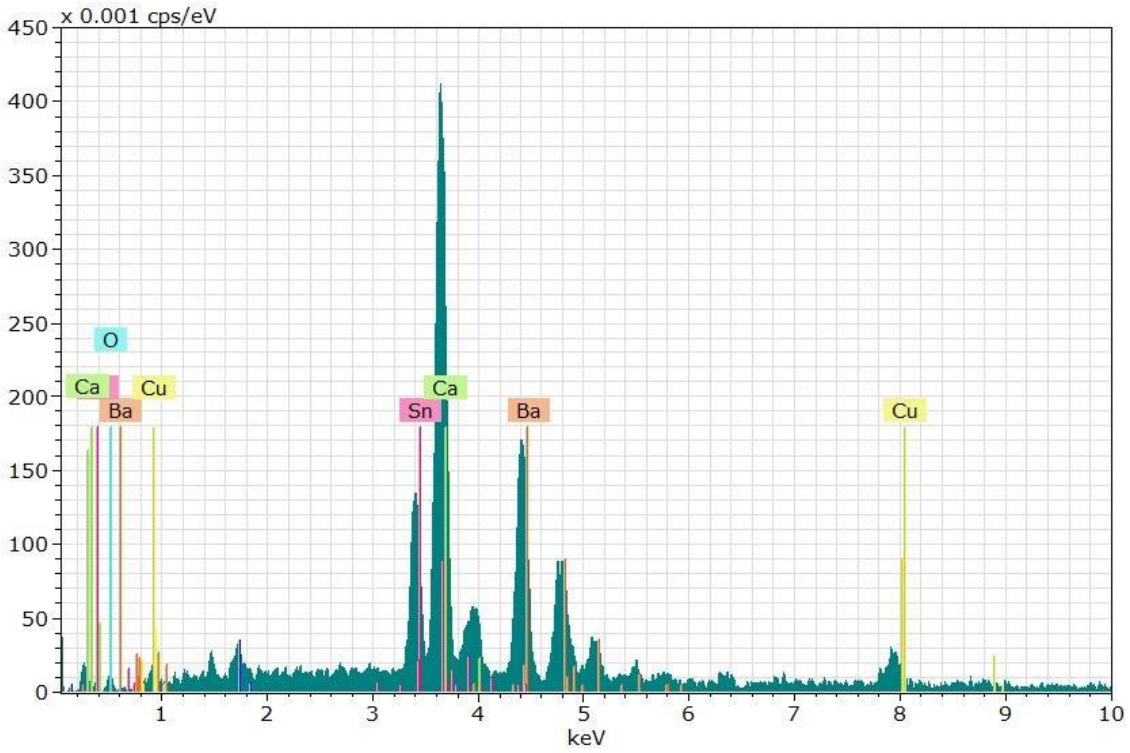

Figure (3-19): EDS spectrum for $Sn_3Ba_4Ca_2Cu_7O_{16+\delta}$

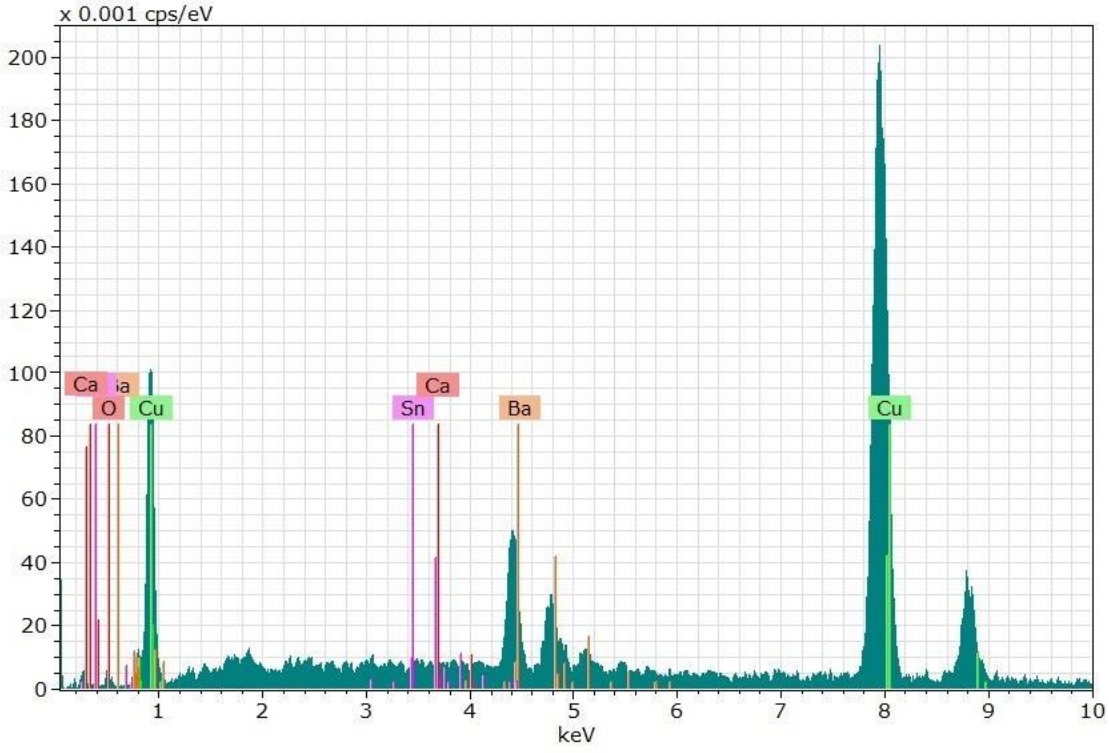

Figure (3-20): EDS spectrum for $Sn_4Ba_4Ca_2Cu_8O_{18+\delta}$

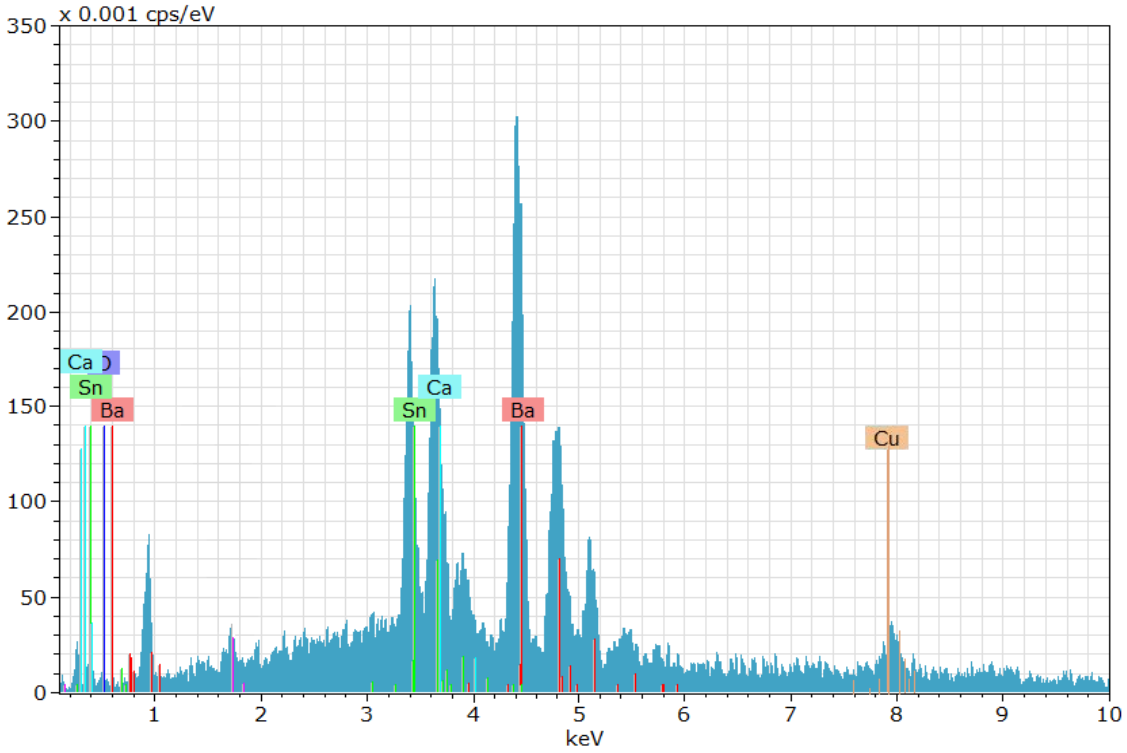

Figure (3-21): EDS spectrum for $Sn_5Ba_4Ca_2Cu_9O_{20+\delta}$

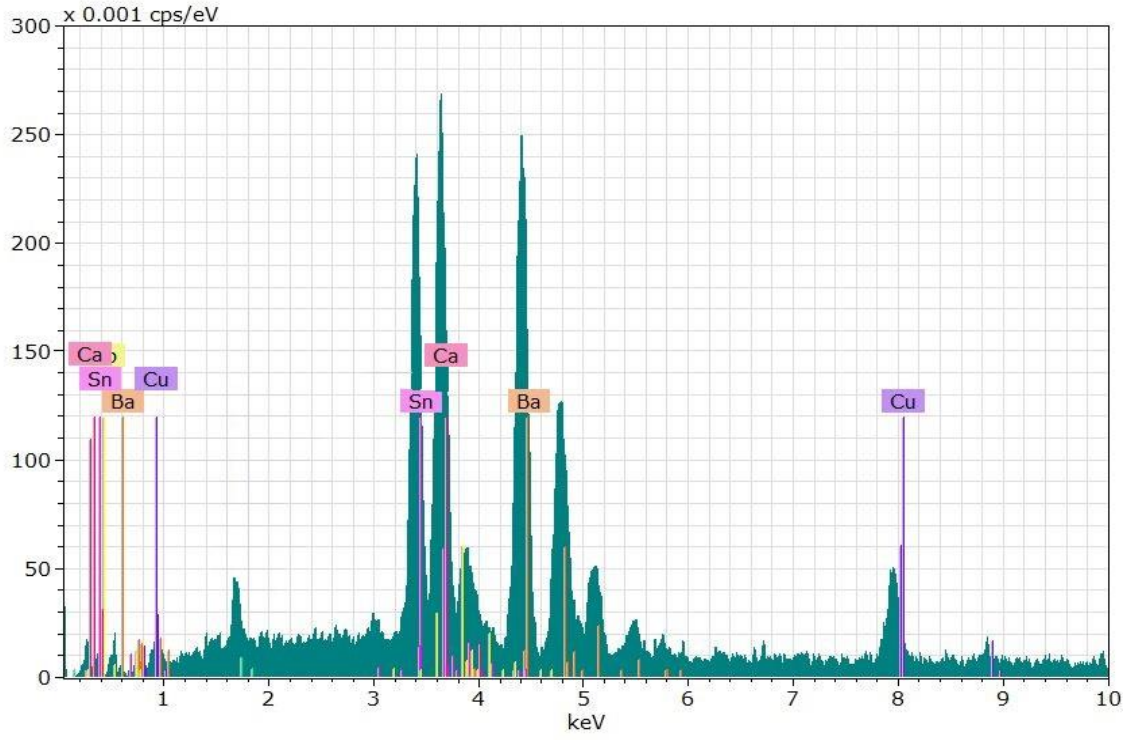

Figure (3-22): EDS spectrum for $Sn_6Ba_4Ca_2Cu_{10}O_{22+\delta}$

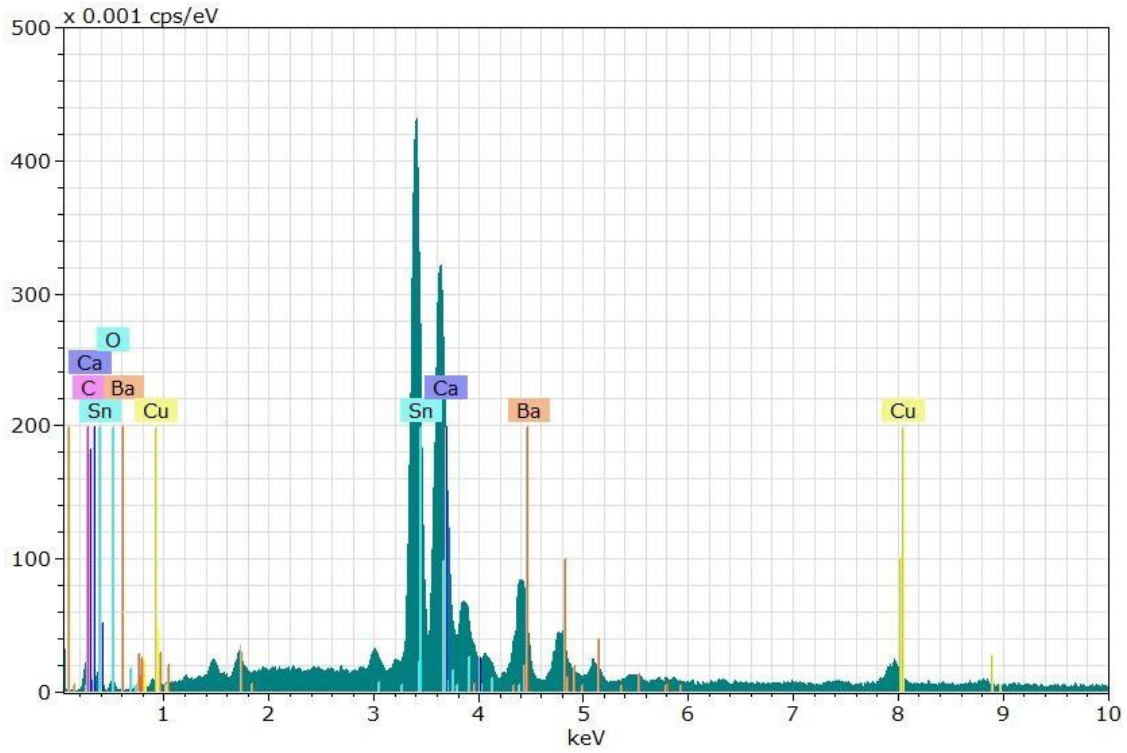

Figure (3-23): EDS spectrum for $Sn_7Ba_4Ca_2Cu_{11}O_{24+\delta}$

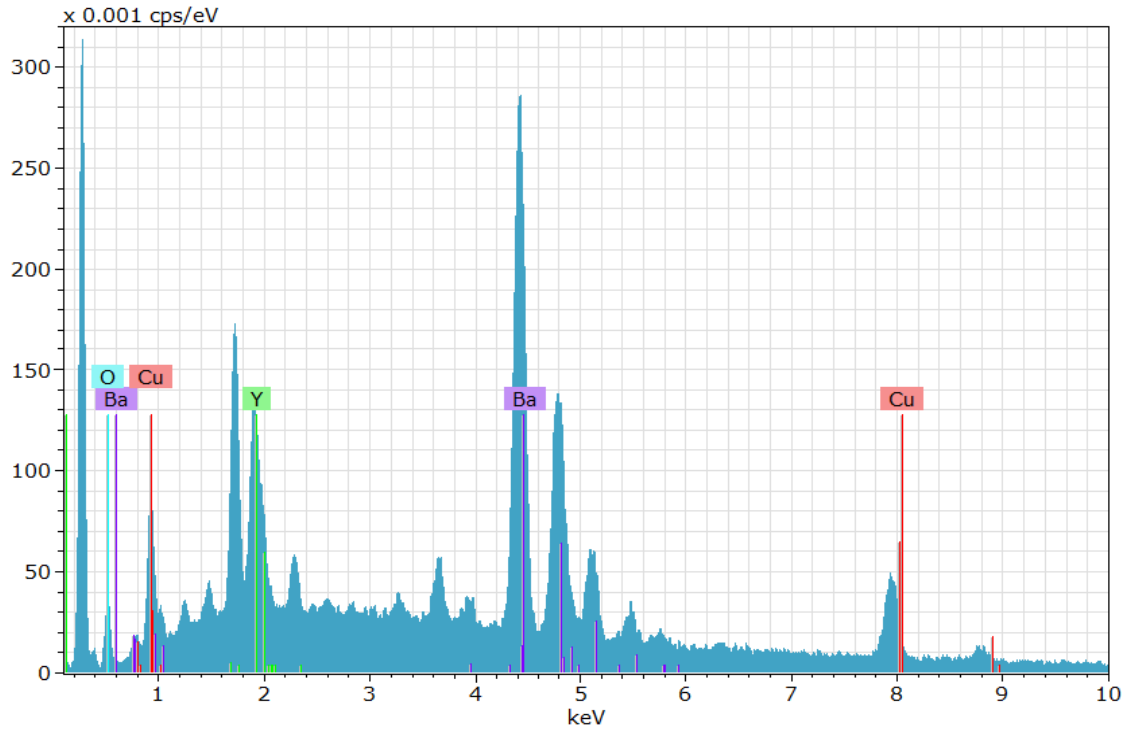

Figure (3-24): EDS spectrum for $Y_3Ba_5Cu_8O_{18+\delta}$

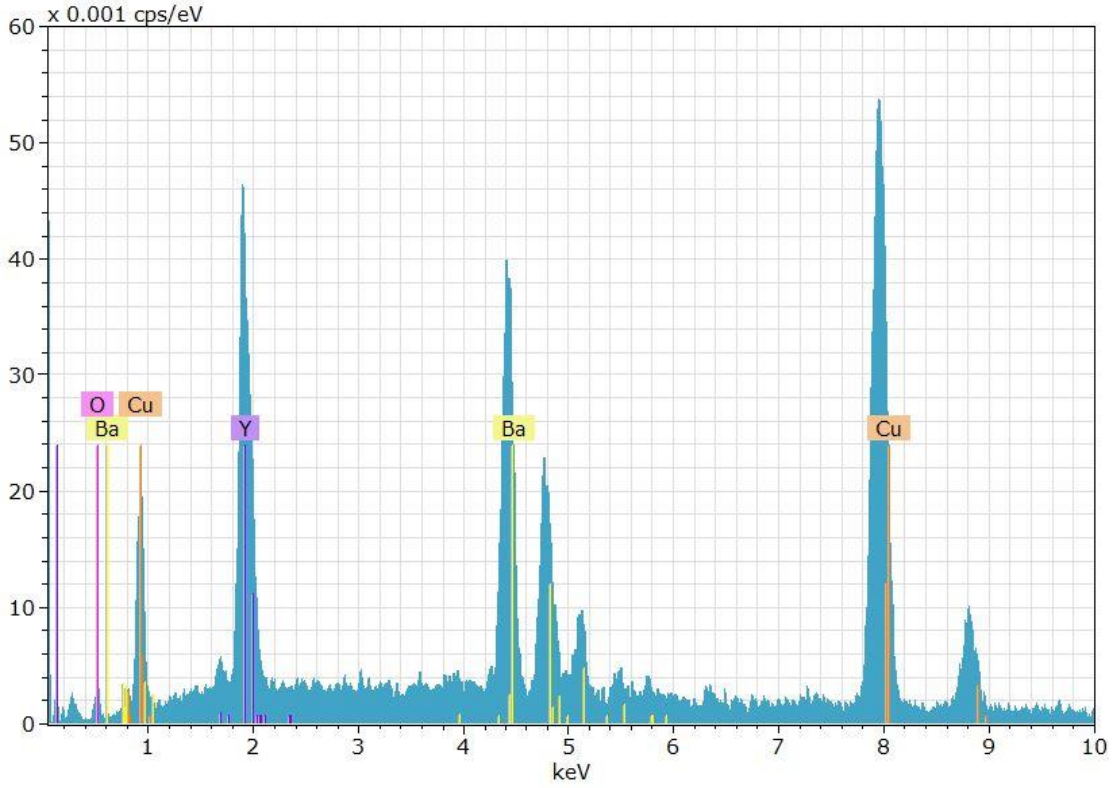

Figure (3-25): EDS spectrum for $Y_5Ba_5Cu_{10}O_{22.5+\delta}$

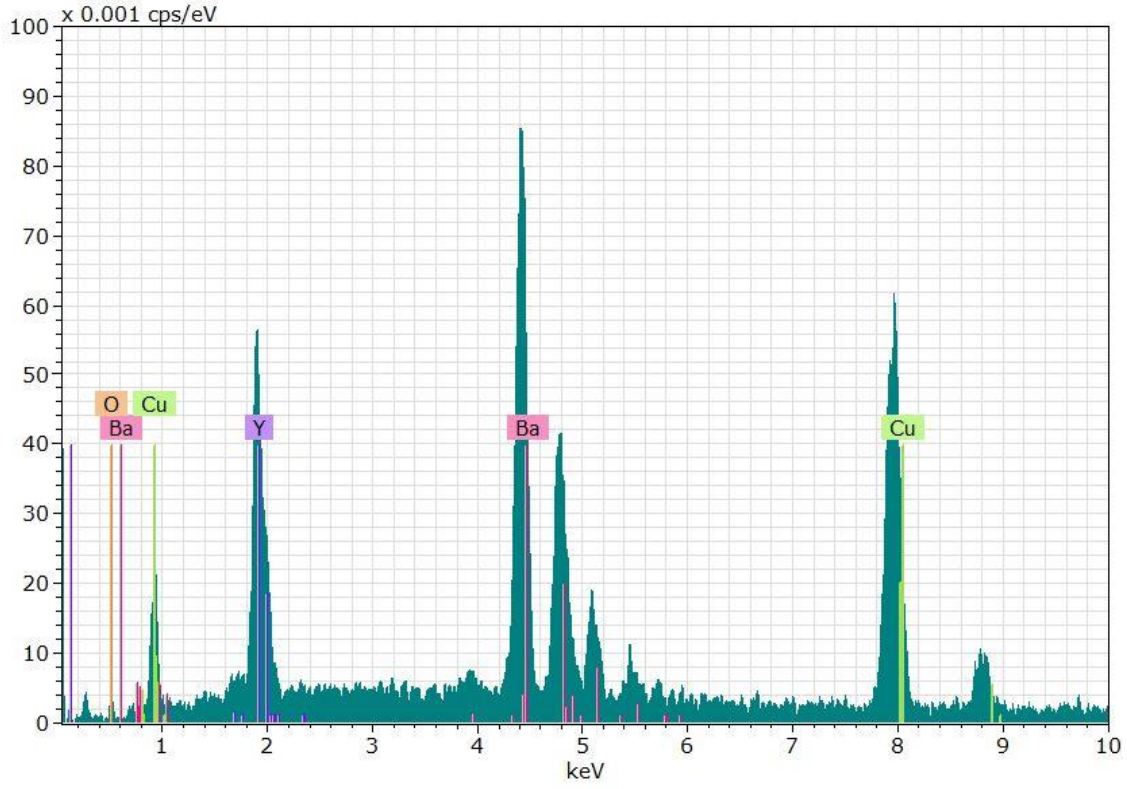

Figure (3-26): EDS spectrum for $Y_7Ba_5Cu_{12}O_{27.5+\delta}$

Chapter Four

Conclusions and future work

4.1 Conclusions

From the results can be summarized the conclusion as follows:

1. Results of electrical resistivity measurements of the $Sn_xBa_4Ca_2Cu_{x+4}O_y$ compounds indicated presence the semiconducting behavior in the temperature range (290 – 110 K) .

2. Results of Iodemetric titration showed an increase in negative charge, which means that the compound is a semiconductor-type p, to increase the number of free carriers (electrons), semiconductors are “doped” with a certain impurities.

3. The emergence of Nano road in x=6 and 7 due to the increased concentration of tin and copper and that needs more development on the experimental procedure to conclude a pure nano roads and apply in the devices

4. The grown phase is Tetragonal structure with elongation in a and c-axis until x=5 as a result of extra insertion of $Cu_{x+4}O_{2x+10}$ layer with in the unit cell. But these parameters go to abrupt decreasing due to shrinkage in the basal plane. That’s attributed to the bending in the bond because O-atoms take the interstitial site with the unit cell

5. The presence of superconductivity, in the composition $Y_nBa_5Cu_{n+5}O_y$ for (n=3, 5, 7), is reasonable in spite of decreasing the critical temperature. That is related to increasing Y-Cu-O layers within the unit cell.

6. The important thing that was noticed form this research is the phase homogeneity created at (n=5, 7) rather than the phase (n=3). This reality was

investigated through XRD analysis during the unknown peaks and diminished at (n=5, 7) and the values of (ΔT_c) are approaching value rather than to (n=3).

7. The last reason is the homogeneity of surface morphology for (n=5, 7) rather than to (n=3). It is possible to conclude that there is ability to presence a new composition of Y-Ba-Cu-O exhibited HTSc.

8. The grown phase is orthorhombic structure with limited increasing in b-axis and sharp increasing in c-axis. That is investigated during much insertion of Y-Cu-O layers within the structure.

4.2 Future Works

1. Searching on the new compositions of yttrium may be give highest temperature.

2. Preparation the SBCCO and YBCO compounds by the sol-gel method and comparable the results with these by solid state reaction.

3. Doping Sn to Y-Ba-Cu-O system and determine the critical temperature.

4. Studying the mechanical properties and phase diagram for the compounds in this research.

5. The searching on the families of superconductor might be record T_c approach to room temperature.

References

1. N.Khare, “Handbook of High-Temperature Superconductor Electronics”, Marcel Dekker, (2003).
2. H. C. Ohanian, Physics, 2nd Edition, WW Norton & co Inc, United Kingdom (1989).
3. G. B. Lubkin, "Power Applications of High- Temperature Superconductors", Physics Today 49, p48, March (1996).
4. K. Fossheim, and A. Sudbø, “Superconductivity Physics and Applications”, John Wiley & Sons Ltd, the Atrium, Southern Gate, Chichester, West Sussex England, (2004).
5. D. Halliday, R. Resnick, J. Walker, "Fundamentals of Physics", 4th Edition, (1994).
6. N.Khare, “Handbook of High-Temperature Superconductor Electronics”, Marcel Dekker, (2003).
7. C. P. Poole Jr., H. A. Farach , R. J. Creswick and R. Prozorov, "Superconductivity", Academic Press is an imprint of Elsevier , Second edition (2007).
8. Z. Yin, "Microscopic Mechanisms of Magnetism and Superconductivity Studied from First Principle Calculations", ph. D. dissertation, University of California, December (2009).
9. K. Fossheim and A. Sudbø, "Superconductivity Physics and Applications", John Wiley & Sons Ltd, England (2004).
10. F. London & H. London, Proc. R. Soc. London A 149, 71(1935).
11. J.Barden, L.N.Cooper and J.R.Schrieffer ; Phys .Rev. V.106,P.62,(1957).
12. B. D. Josephson. Physics Letters, 1:251, (1962).
13. J. G. Bednorz and K. A. M¨uller, Z. Phys. B64, 189 (1986).
14. H. Kamimura, H. Ushio, S. Matsuno and T. Hamada, "Theory of Copper Oxide Superconductors", Springer-Verlag, Germany (2005).

15. M. K. Wu, J. R. Ashburn, C. J. Torng, P. H. Hor, R. L. Meng, L. Gao, Z. J. Huang, Y. Q. Wang, and C. W. Chu, "Superconductivity at 93 K in a new mixed-phase Y-Ba-Cu-O compound system at ambient pressure" Phys. Rev. Lett. 58, 908 (1987).
16. H. Maeda, Y. Tanaka, M. Fukutomi, and T. Asano: Jpn. J. Appl. Phys., V.27, L209, (1988).
17. Z. Z. Sheng, and A. M. Hermann, V. 332, N. 6159, P.55, (1988).
18. A. Schilling, M. Gantoni, H. V. Niessen and H. R. Otl: phys. V.215, N.1, P.11, (1993).
19. J. B. Trenholme, "Superconducting Proximity Effect Currents in Indium above Its Transition Temperature", PH. D. dissertation, California Institute of Technology Pasadena, California (1970).
20. D. Dew-Hughes, "The critical current of superconductors: an historical review", American Institute of Physics, Oxford OX1 3PJ, UK (2001).
21. A. Maqsood & M. Maqsood," Proceeding of International Workshop held at Ragshahi University"; Bangladesh, edited by AKMA Islam, (1996).
22. W. Meissner and R. Oschenfeld, *Naturwiss.* 21, 787 (1933).
23. J. W. Lynn, "High Temperature Superconductivity", Springer-Verlag, (1990).
24. S. Fujita and S. Godoy, "Quantum Statistical Theory of Superconductivity", Kluwer Academic Publishers, (2002).
25. M. Sjostrom, "Hysteresis modelling of high temperature superconductors", PH. D. Dissertation, N.2372, Sweden (2001).
26. H. P. Myers; "Introductory to Solid State physics", (Superconductivity Ch.13), Taylar and Francis (1990).
27. M. A. Omer, "Elementary Solid State Physics Principles and Applications", ch.10, Addison-Wesley, (1975).
28. S. M. Shapiro, J. D. Axe, and G. Shirane, Phys. Rev. B 12, 4899 (1975).
29. L. Ginzburg and D. L. Landau, Zh. Eksp. Theor. Fiz. 20, 1064- 1082 (1950).

30.J. Bardeen, L. Cooper, and J. Schrieffer, Phys. Rev. 108, 1115 (1951).

31. L.N. Cooper, Phys. Rev. 104, 1189 (1956).

32. G. Berdiyorov, "Vortex Structure and Critical Parameters in Superconducting Thin Films with Arrays of Pinning Centers", Antwerpen (2007).

33. P. Aynajian, "Electron–Phonon Interaction in Conventional and Unconventional Superconductors", Springer Theses Recognizing Outstanding Ph.D. Research, Germany (2010).

34. K. S. Aleksandrov, A. D. Vasil'ev, S. A. Zvegintsev, S. N. Krivomazov, M. I. Petrov, and B. P. Khrustalev, "Tin-based high-temperature superconductor", American Institute of physics, No. 12, 658-660 (1989).

35. J. James, O.B.S. Kumar, S. S. Kumar, P. P. Rao, and K.V.O. Nair, "Nanoparticles of Ba_2MSnO_{6-x} (M=Ce, La and Nd; x=0 or 0.5): a new group of complex perovskite oxides", Materials Letters 57, 3641– 3647, India (2003).

36. T. Firdous and N. A. Khan, "Sn doped $Cu_{0.5}Tl_{0.5}Ba_2Ca_2Cu_{3-y}Sn_yO_{10-\delta}$ superconductors: Effect on the diamagnetism and phonon modes", Journal of Applied Physics 106, 083901, Pakistan (2009).

37. M. Irfan, S. Khan, N. Hassan, and N. A. Khan, "Fluctuation-Induced Conductivity of $Cu_{0.5}Tl_{0.5}Ba_2Ca_2Cu_2MO_{10-\delta}$ (M = Si, Sn, Ge) Superconductors", J Supercond. Nov Magn 22: 769–774, DOI 10.1007/s10948-009-0495-4, Pakistan (2009).

38. T. Firdoss, A.A. Khurram, and N. A. Khan, "AC Response of $Cu_{0.5}Tl_{0.5}Ba_2Ca_2Cu_{3-x}Sn_xO_{10-\delta}$ Superconductor", J Supercond Nov Magn 23: 325–328, DOI 10.1007/s10948-009-0533-2, Pakistan (2010).

39. M. Mumtaz, N. A. Khan, and R. Nawaz, "Superconductivity and Electron–Phonon Interaction in $Cu_{0.5}Tl_{0.5}Ba_2Ca_2Cu_{3-y}M_yO_{10-\delta}$ (M = 0, Si, Ge, Sn, and y = 0, 1)", J Supercond Nov Magn 23: 565–569, DOI 10.1007/s10948-010-0768-y, Pakistan (2010).

40. N. A. Khan, N. Hassan, S. Nawaz, B. Shabbir, S. Khan, and A. A. Rizvi, "Effect of Sn substitution on the para conductivity of polycrystalline $Cu_{0.5}Tl_{0.5}Ba_2Ca_2Cu_{3-y}Sn_yO_{10-\delta}$ superconductors", Journal of Applied Physics 107, 083910 , Pakistan (2010).
41. S. Sato, K. Kim, M. Kato, T. Noji, and Y. Koike, "Synthesis of a new superconductor $EuSr_2Cu_2(Ta,Sn)O_{8-y}$", Physica C 504 (1-3), Japan (2014).
42. R. N. Steinberg, "Synthesis and characterization of Yttrium-Barium-Copper-Oxide thin films", Ph. D. Dissertation, Yale university, (1992).
43. A. Aliabadi, Y. Akhavan, and M. Akhavan, "A new Y-based HTSC with Tc above 100 K", physica c, Iran (2009).
44. T. Kruaehong, S. Sujinnapram, P. Udomsmuthirun, T. Nilkamjon, and S. Ratreng, "Structural and superconducting properties of $Y_3Ba_5Cu_8O_{18}$", 9th International Conference on Facture & strength of solids, Korea (2013).
45. P. Udomsmuthirun, T. Kruaehong, T. Nilkamjon, and S. Ratreng, "the new superconductors of YBaCuO materials", J Supercond Nov Magn, Thailand (2010).
46. R.V. Vovk, N.R.Vovk , A.V.Samoilov , I.L.Goulatis , and A.Chroneos, "Effect of long aging on the resistivity properties of optimally doped $YBa_2Cu_3O_{7-\delta}$ single crystals", Solid StateCommunications170, 6–9, United Kingdom (2013).
47. K. Nakazato, M. Muralidhar, M.R. Koblischka, and M. Murakami, "Fabrication of bulk Y–Ba–Cu–O superconductors with high critical current densities through the infiltration-growth process", Cryogenics 63, 129–132, Japan (2014).
48. C. Wu, G. Zhao, and F. Qiao, "Characteristics of $YBa_2Cu_3O_{7-x}/SrTiO_3/YBa_2Cu_3O_{7-x}$ films formed by chemical solution deposition", Ceramics International 40, 13145–13150, China (2014).

49. M.K. Ben Salem, A. Hamrita, E. Hannachi, Y. Slimani, M. Ben Salem , and F. Ben Azzouz, "The study on SiO_2 nanoparticles and nanowires added YBCuO: Microstructure and normal state electrical properties", Physica C 498, 38–44, Tunisia (2014).
50. S.B. Guner , O. Gorur , S. Celik , M. Dogruer , G. Yildirim , A. Varilci , and C. Terzioglu , "Effect of zirconium diffusion on the microstructural and superconducting properties of $YBa_2Cu_3O_{7-\delta}$ superconductors", Journal of Alloys and Compounds 540, 260–266, Turkey (2012).
51. S. Khene, M.Gasmi, and G.Fillion, "Phase transitionin$YBa_2Cu_3O_{7-\delta}$ and $YBa_2Cu_3O_{7-\delta}/Y_3Fe_5O_{12}$ nanoparticles at low temperatures and high fields", Journal of Magnetism and Magnetic Materials 373,188–194, Algeria (2015).
52. S. Alikhanzadeh-Arani, M. Salavati-Niasari , and M. Almasi-Kashi, "Influence of the utilized precursors on the morphology and properties of $YBa_2Cu_3O_{7-\delta}$ superconducting nanostructures", Physica C 488, 30–34, Iran (2013).
53. L.A. Klinkova, and V.I. Nikolaichik, "Nanostructural inhomogeneity of $YBa_2Cu_3O_7$", Physica C 506, 33–39, Russia (2014).
54. A. Zalga, J. Reklaitis , E. Norkus , A. Beganskiene , and A. Kareiva, "A comparative study of $YBa_2Cu_4O_8$ (Y-124) superconductors prepared by a sol–gel method", Chemical Physics, Lithuania (2006).
55. D. Giri, "Study of Electrical Transport Property of $YBa_2Cu_3O_{7-\delta}$ + x $BaSnO_3$ Superconductor", ROLL NO: 411PH2093, National Institute of Technology, Rourkela.
56. P. Rani, A. Pal, and V.P.S Awana, "High field magneto-transport study of $YBa_2Cu_3O_7$:Ag_x (x = 0.00–0.20)", Physica C 497, 19–23, India (2014).
57. S. Naji, E. Al-Shakarchi, and M. Makadsi, "Resistivity Measurements of HTSc Compound Using Van der pauw Technique", proceedings of the first scientific conference, Vol. 1, pp. 275-279, 1997.

58. H. Nobumasa, K. Shimizu, Y. Kitano, and T. Kawai, J. Appl. Phys.,V.27, P.846, (1988).
59. A.Manthiran,J.S.Swinnea,Z.T.Sui,"J.Am.Chem.Sov.",109, 22, 6667, (1987).
60. T. Kruaehong; Int. J. Phys. Sci., vol. 9, no.16, p. 360, (2014).
61. K. Srinivasan, G. Thomas C, P. Padaikathan, N.V.Ashoka; Int. J. of Engin. Res. and Appl. (IJERA), Vol. 3, no. 1, p. 927, (2013).
62. M. Thoma, Y. Shi, T. Dennis, J. Durrell, and D. Cardwell, "Effect of Y-211 particle size on the growth of single grain Y–Ba–Cu–O bulk superconductors", Journal of Crystal Growth 412, 31–39, UK (2015).
63. G. Alecu, "The Morphology of Some YBCO Superconductor Materials", Splaiul Unirii 313, 74204, Romania (2001).

الخلاصة

يتضمن البحث تحضير ودراسة المركبات $Sn_xBa_4Ca_2Cu_{x+4}O_y$ و $Y_nBa_5Cu_{n+5}O_y$ مع قيم مختلفة لكل من x و n، حيث (x=3, 4, 5, 6, 7) و (n=3, 5, 7) بطريقة تفاعل الحالة الصلبة من خلال تطعيمها بالأوكسجين في أنبوب كوارتز وإمكانية استنتاج مواد فائقة التوصيل.

وتمت دراسة هذه المركبات السيراميكية بواسطة تأثير ميزنر وقياس كمية الأوكسجين المضاف خلال عملية التلبيد من خلال الطريقة الكيميائية (المعايرة بإستخدام اليود)، وتحليل العينات بواسطة حيود الاشعة السينية لدراسة التركيب البلوري وايجاد قيم ثوابت الشبيكة، وقياس المقاومة الكهربائية كدالة لدرجة الحرارة بتقنية (Van der Pauw).

ولقد أظهرت نتائج المقاومة لنظام Sn-Ba-Ca-Cu-O بأنه مركب شبه موصل حيث تزداد المقاومة بإنخفاض درجة الحرارة ووجد أن أقل مقاومة بدرجة حرارة الغرفة عند x=6 وأعلاها عند x=4. بينما نتائج نظام Y-Ba-Cu-O أظهرت بأنها مركبات فائقة التوصيلية بدرجات حرارية حرجة عالية، حيث كانت قيمة درجة الحرارة الحرجة عند (x=3, 5, 7) هي (T_c=113.6, 113, 105 K) على التوالي.

ومن خلال نتائج تحليلات حيود الأشعة السينية (XRD) للمركب $Sn_xBa_4Ca_2Cu_{x+4}O_y$ تبين بأن له تركيب رباعي الأطوار (tetragonal) لجميع قيم x وأن قيمة البعد البلوري c-axis تزداد بزيادة x حتى تصل أعلى قيمة عند x=5 ثم تتناقص عند x=6, 7 . أما بالنسبة للمركب السيراميكي $Y_nBa_5Cu_{n+5}O_y$ فقد أظهرت النتائج أن له تركيب معيني متعامد المحاور (orthorhombic) لجميع قيم n أيضا، وقد وجد أن بزيادة تركيز اليتريوم وعدد الطبقات CuO_2 تزداد قيم الأبعاد البلورية b & c-axis.

من جهة أخرى، أظهرت نتائج التحليل بالمجهر الألكتروني الضوئي وجود تركيب نانوي عند $Sn_6Ba_4Ca_2Cu_{10}O_{22}$ و $Sn_7Ba_4Ca_2Cu_{11}O_{24}$ بحدود (100-300 nm) في حين ظهر التركيب المايكروي لبقية مركبات ال Sn-family. أما المركب $Y_3Ba_5Cu_8O_{18}$ ظهرت الحبيبات عشوائية وكبيرة مقارنة بـ $Y_5Ba_5Cu_{10}O_{22.5}$و $Y_7Ba_5Cu_{12}O_{27.5}$ مع غياب المسافات البينية تقريبا. وكانت نتائج ال EDS متوافقة مع القيم النظرية للعناصر من المعادلة الكيميائية.

جمهورية العراق
وزارة التعليم العالي والبحث العلمي
جامعة النهرين
كلية العلوم
قسم الفيزياء

تحضير ودراسة المركبات $Sn_xBa_4Ca_2Cu_{x+4}O_y$ و $Y_nBa_5Cu_{n+5}O_y$

رسالة
مقدمة إلى كلية العلوم/ جامعة النهرين
كجزء من متطلبات نيل درجة الماجستير في علوم الفيزياء

من قِبَلْ
رؤى فخري هادي
بكالوريوس 2010

إشراف
الأستاذ الدكتور عماد خضير الشكرجي

رمضان ١٤٣٦هـ **تموز** ٢٠١٥ م